https://doi.org/10.5194/egusphere-2026-2879
Preprint. Discussion started: 11 June 2026

Projected changes in African Easterly Waves and rainfall events in West Africa with kilometre-scale global coupled simulations

Jerry Raj[1], Elsa Mohino[1], Belén Rodríguez-Fonseca[1,2], Teresa Losada[1], Thomas Rackow[3,4], and Tobias Becker[3]

[1]Departamento de Física de la Tierra y Astrofísica, Universidad Complutense de Madrid, Madrid, Spain
[2]Geosciences Institute, CSIC-UCM, Madrid, Spain
[3]European Centre for Medium-Range Weather Forecasts (ECMWF), Bonn, Germany
[4]Alfred Wegener Institute, Helmholtz Centre for Polar and Marine Research (AWI), Bremerhaven, Germany

Correspondence: Jerry Raj (jraj@ucm.es)

Abstract. African easterly waves (AEW) are a key modulator of West African rainfall variability with impacts on tropical cyclon activity. However, climate change projections of AEW show contrasting results, underpinned by the coarseness of some simulations and the lack of consistency with surface conditions in others. Here we analyse the performance and projected changes in 3-5 day AEWs using two 30-yr long simulations consistent with historical (1990-2019) and near-future climate conditions (2020-2049) by IFS-FESOM model at kilometer scale horizontal resolution. We show that the model captures the spatial structure and energetics of AEW with reasonable accuracy, although it overestimates associated precipitation variability. The model projects an intensification of AEW activity over land associated with enhanced barotropic and baroclinic conversion and stronger diabatic generation of eddy available potential energy. Over the central and eastern Sahel, the model projects a shift towards more extreme rainfall events and fewer moderate ones, with an overall enhancement of rainfall. This response is not exclusively related to AEW activity, as a similar response is observed when AEW activity is low. Conversely, over the westernmost Sahel, the projected drying is related to a decrease in extreme events during AEW days and in moderate events during non-AEW days. Over eastern Africa, where AEWs originate, the simulated increase in the reversal of the meridional potential vorticity - caused by the increase in static stability as a response to tropical climate warming - and the enhancement of upstream convective variability set the scene for more frequent and stronger seeding disturbances for AEWs. These results underline the importance of improving AEW representation in climate models to enhance seasonal forecasting, early warning systems, and adaptation strategies in the region.

1 Introduction

West Africa experiences a complex and highly variable rainfall regime governed by interactions between large-scale climate drivers and mesoscale processes. Key drivers of WA rainfall variability are African Easterly Waves (AEW), particularly the 3- to 5-day wave modes that modulate convective activity. AEWs typically manifest at 600 to 700 hPa on either side of the African Easterly Jet (AEJ) and play a key role in the high-frequency variability of precipitation associated with the West African Monsoon (WAM), significantly contributing to annual rainfall in the Sahel. AEWs are fundamental for the development

https://doi.org/10.5194/egusphere-2026-2879
Preprint. Discussion started: 11 June 2026

of Mesoscale Convective Systems (MCSs) and squall lines in West Africa, accounting for a substantial portion of the annual precipitation in the region (Fink and Reiner, 2003; Janiga and Thorncroft, 2014). Approximately 40% of MCSs (Fink and Reiner, 2003) are related to AEWs, and these systems contribute nearly 80% to the total Sahelian rainfall (Liu et al., 2019; Nesbitt et al., 2006).

AEWs are also instrumental in the formation of Atlantic tropical cyclones. The westward-propagating synoptic-scale disturbances originate over tropical eastern Africa and extend into the Atlantic, serving as precursors to tropical cyclogenesis and facilitating the transport of Saharan dust across regions. Approximately 60% of all hurricanes and 80% of the major hurricanes originate from AEW disturbances (Landsea, 1993). Southern-track AEWs are more favorable for hurricane development due to their higher moisture content, while northern-track AEWs, which are relatively drier, play a lesser role in cyclogenesis (Dieng et al., 2017). The impact of AEWs extends beyond West Africa, influencing climate patterns along their Atlantic pathways, making their future evolution a critical research topic. For instance, Bercos-Hickey and Patricola (2024) found that the recent observed trend towards higher tropical cyclone activity is associated with stronger and more frequent AEWs.

Several studies have examined projected changes in AEWs under climate change. Analysis using CMIP-type models suggests that northern AEWs (15–25°N) may strengthen in response to increased radiative forcing, which could lead to more intense and frequent extreme rainfall events (Skinner and Diffenbaugh, 2014; Akinsanola et al., 2025; Martin and Thorncroft, 2015). Martin and Thorncroft (2015) document more than a 30% increase in summer eddy kinetic energy (EKE) over land. In contrast, the southern track does not show a consistent response, some models projecting a clear reduction in wave activity with weak waves decreasing and strong waves increasing (Brannan and Martin, 2019; Hannah and Aiyyer, 2017). Projections indicate a decline in AEW activity in late spring and early summer but an intensification between July and October, although discrepancies exist between higher and lower resolution models (Martin and Thorncroft, 2015).

Traditional CMIP-type climate models struggle to capture AEWs and related rainfall extremes due to their coarse resolution and biases in simulating the regional-scale convective dynamics (Ruti and Dell'Aquila, 2010). Ruti and Dell'Aquila (2010) demonstrated that CMIP3 models exhibit a wide variety of behaviours in reproducing AEW synoptic features, with significant inter-model spread in the amplitude and spatial distribution of wave variance over West Africa. This bias persists into CMIP5, where Martin and Thorncroft (2015) found that models simulate excessive eddy kinetic energy over the continent alongside deficient rainfall, and fail to accurately couple AEWs with precipitation. A potential way to increase resolution is by means of regional climate modelling. However, analyses show contrasting results. Some regional climate models (RCMs) project an overall reduction in AEW activity across the region (Kebe et al., 2020), while Bercos-Hickey and Patricola (2021) report a 20 % increase in eddy kinetic energy (EKE). Another study with a global atmospheric model run at high resolution ($\sim$ 25 km) also suggests an increase in the precipitation and intensity of circulation related to AEWs (Raj et al., 2023).

Projected changes in AEW tracks include significant northward expansion (Raj et al., 2023), higher-altitude strengthening of southern tracks (Bercos-Hickey and Patricola, 2021), and shifts along the Intertropical Front (Skinner and Diffenbaugh, 2014). One study reports a 21% rise in track count (Bercos-Hickey and Patricola, 2021), and another links increased AEW strength to a higher likelihood of tropical cyclone development (Bercos-Hickey et al., 2023). Núñez Ocasio et al. (2025), using a novel

https://doi.org/10.5194/egusphere-2026-2879
Preprint. Discussion started: 11 June 2026

storm-resolving regional model under a pseudo-global warming framework, found that AEWs over Africa are projected to become significantly more intense, wetter, and with greater water vapor content in a warmer climate.

Regarding the potential contributors to the projected change in AEW activity, some works suggest an increase in baroclinic and barotropic energy conversions, enhancing EKE (Bercos-Hickey and Patricola, 2021; Akinsanola et al., 2025). Raj et al. (2023) indicate heightened AEW intensity driven by stronger baroclinic overturning and increased eddy available potential energy, and Skinner and Diffenbaugh (2014) associate enhanced AEW strength with amplified regional temperature gradients and increased convergence. In addition, intensified AEW-associated precipitation and modified monsoon flow appear to contribute to changes in AEW dynamics (Skinner and Diffenbaugh, 2014). However, the energy sources driving AEW growth and intensification are highly sensitive to the model parameterizations used. Early studies suggested that AEWs derive energy primarily from barotropic conversion associated with AEJ shear, while more recent research has highlighted the role of diabatic heating and baroclinic conversion (Diaz and Aiyyer, 2013). Convection has also been highlighted as a potential contributor driving biases in AEW simulation (Elless and Torn, 2018). In this way, the impact of climate change on these energy conversions remains an open question.

Moreover, AEWs originate in East and Central Africa, with topographic features such as the Ethiopian Highlands, Marrah Mountains, and Guinea Highlands playing a crucial role in their initiation and propagation. The representation of these features in models is essential for accurately simulating AEWs. Coarse-resolution models often struggle to maintain AEW propagation across West Africa and into the Atlantic due to their inability to resolve key topographic influences, particularly over the Guinea Highlands (Martin and Thorncroft, 2015). Studies have shown that these regions provide diabatic heating that reinforces AEWs, facilitating their westward movement (Ventrice et al., 2012). However, improving topographic resolution alone may not be sufficient, as convective parameterization is also a major factor in AEW simulation.

While RCMs or atmospheric models run at similar high-resolution configurations have been employed to address some of the limitations of coarse-grid global coupled models, they often rely on boundary conditions, leading to inconsistencies in sea surface temperature (SST) patterns and their influence on AEW dynamics (Sylla et al., 2013). In contrast, in this work we analyse 30-year-long global coupled simulations run at 9 km horizontal resolution in the atmosphere and up to 5 km in the ocean from the nextGEMS EU project (Segura et al., 2025). These nextGEMS simulations offer a unique opportunity to evaluate the impact of climate change on AEW and related precipitation with a self-consistent and high-resolution model, which is potentially more capable of simulating the delicate interplay of convection, wind dynamics, and topographical features that are key to the initiation and propagation of AEW.

2 Data

2.1 Observations and Reanlyses

This study utilises three datasets to validate the IFS historic simulations: the Climate Hazards InfraRed Precipitation with Stations (CHIRPS), the Multi-Source Weighted-Ensemble Precipitation (MSWEP), and the fifth-generation ECMWF reanalysis (ERA5). CHIRPS is a quasi-global precipitation dataset that combines satellite imagery with in situ station data to produce

https://doi.org/10.5194/egusphere-2026-2879
Preprint. Discussion started: 11 June 2026

high-resolution daily and monthly precipitation estimates. It covers the period from 1981 to the present with a spatial resolution of 0.05° (Funk et al., 2015). MSWEP is a global precipitation dataset that merges multiple data sources, including gauge observations, satellite estimates, and reanalysis output, and spans from 1979 to the present, at a 0.1° spatial resolution (Beck et al., 2019). Daily precipitation fields from CHIRPS and MSWEP are used to validate the IFS simulation. ERA5 has a spatial resolution of approximately 31 km (0.25°) and spans from 1950 to the present (Hersbach et al., 2020). Various atmospheric fields from ERA5 are used in the study. For consistency with the simulations, we used 1990-2019 period for all three datasets.

2.2 Model Experiments

In this work, we use model experiments from the Horizon 2020 nextGEMS project (https://nextgems-h2020.eu). Throughout several model development cycles, the project's goal was to develop storm- and eddy-resolving models and apply them for the first time on climate timescales. Among the different nextGEMS simulations, we focus here on the 30-year-long production simulations with IFS-FESOM (Segura et al., 2025). The simulations were run at 9 km horizontal resolution for the atmosphere component (TCo1279-NG5 grid combination) and up to 5 km in the ocean, which can be considered eddy-resolving in large parts of the global ocean (Rackow et al., 2025). The IFS-FESOM production simulations consist of a set of twin experiments that differ only in the ocean-atmosphere initial state and the boundary conditions (greenhouse gases, ozone, and aerosols), consistent with the historical period (1990-2019) and following the SSP3-7.0 scenario (O'Neill et al., 2016) for the 2020-2049 period, hereafter named 'historical' and 'future' simulations, respectively. The ocean has been spun up with ERA5 atmospheric forcing (Hersbach et al., 2020) in stand-alone mode, for a duration of 5 years, before the respective start date of the coupled historical (1 January 1990) and future simulations (20 January 2020). Additionally, the ocean state of the historical simulation has undergone 2 years of coupled spinup before starting production in 1990. While 5 years of ocean spinup may seem short, Rackow et al. (2025) had noticed little surface drift of the coupled IFS-FESOM system in Cycle 3 of the nextGEMS development cycle with the identical eddy-resolving ocean grid, and it was therefore decided to stick to 5 years of standalone spinup for better comparability. The atmospheric initial conditions are from the IFS operational analysis for 1 January 1990 and 20 January 2020, respectively. Aerosols are fixed in time for the scenario. Both the historical and future simulations use a weakly active convection scheme, via a reduced cloud base mass flux. In other words, this lends more weight to explicit convection than using a fully active deep convection parameterisation (Rackow et al., 2025). The simulations store their output on the HEALPix grid. Other details can also be found on the easy.gems documentation page (https://easy.gems.dkrz.de/DYAMOND/NextGEMS/prefinal.html).

3 Methods

3.1 Identification of AEWs

The study focuses on 3-5 day AEWs during boreal summer, and the waves are extracted from the mean field using a Butterworth bandpass filter of the same period applied to meridional wind at 700 hPa over the June–September (JJAS) season. This pressure

https://doi.org/10.5194/egusphere-2026-2879
Preprint. Discussion started: 11 June 2026

level is commonly used for AEW analysis, as supported by previous studies (Carlson, 1969; Berry and Thorncroft, 2005, 2012; Kiladis et al., 2006). Composite anomalies for the wave initiation day (day 0) were created based on wind and rainfall anomalies corresponding to the top and bottom deciles of the filtered 700 hPa meridional wind values at the base point located at 1°W and 11.5°N. Circulation and precipitation anomalies were then computed for days –4, –2, +2, and +4 relative to the wave initiation. This approach aligns with the methodology used by Crétat et al. (2015) for constructing composite anomalies. A similar method is used to identify AEW and non-AEW days. To isolate AEW days, the JJAS 700 hPa filtered meridional wind at the same base point was used. AEW days were identified as those corresponding to wind anomalies exceeding the 90th percentile or falling below the 10th percentile of the filtered distribution. The magnitude of the wind taken as the threshold for each percentile was calculated from the historical simulation and applied to the projection. A ±2-day temporal offset was applied to account for wave evolution, and duplicate days were excluded to avoid redundancy. The resulting set of unique days was classified as AEW days, while all remaining days within the JJAS season were designated as non-AEW days.

3.2 Contributions to future changes in rainfall

The seasonal total precipitation can be decomposed into the part falling during AEW and that falling during non-AEW days to identify the contribution of each term to the future change in precipitation as follows:

$$P = P_A * n_A + P_N * n_N \tag{1}$$

where P - total precipitation (mm/day)

P_A - precipitation during AEW days (mm/day)

P_N - precipitation during Non AEW days (mm/day)

n_A - fraction of total days which are AEW days

n_N - fraction of total days which are non-AEW days

Similarly,

$$P^h = P_A^h * n_A^h + P_N^h * n_N^h \tag{2}$$

$$P^f = P_A^f * n_A^f + P_N^f * n_N^f \tag{3}$$

where h and f represent historical and future simulations respectively.

From 2 and 3, future change in precipitation can be written as:

$$\Delta P = \underbrace{n_A^h \cdot \Delta P_A + n_N^h \cdot \Delta P_N}_{(1)} + \underbrace{(P_A^h - P_N^h) \cdot \Delta n_A}_{(2)} + \underbrace{(\Delta P_A - \Delta P_N) \cdot \Delta n_A}_{(3)} \tag{4}$$

where $\Delta P = P^f - P^h$ is the total change in precipitation, $\Delta P_A = P_A^f - P_A^h$ is the change in the mean precipitation during AEW days, $\Delta P_N = P_N^f - P_N^h$ the change in precipitation during the non-AEW days and $\Delta n_A = n_A^f - n_A^h$ is the change in the fraction of AEW days, which is equal to the minus change in the fraction of non-AEW days ($-\Delta n_N$).

https://doi.org/10.5194/egusphere-2026-2879
Preprint. Discussion started: 11 June 2026

On the right-hand side of 4, the first term represents the contribution from changes in precipitation occurring both during AEW and non-AEW days. The second term captures the contribution from the change in the fraction of AEW days from the historical to the projection. The third term accounts for the cross-product term, which is expected to be small, as it takes into account modifications that come from both changes in the mean precipitation during AEW and non-AEW days and changes in the fraction of AEW days.

3.3 Eddy kinetic energy sources and transformations

Eddy kinetic energy (EKE) is a measure of synoptic-scale variability, and increased EKE values are often associated with stronger or more frequent AEWs. EKE is computed as

$$EKE = \frac{1}{2}(u'^2 + v'^2) \tag{5}$$

where u' and v' represent the 3–5 day bandpass-filtered zonal and meridional wind components.

To examine the factors contributing to changes in the EKE, we follow previous works (e.g. Hsieh and Cook, 2007; McCrary et al., 2014) and calculate the relevant energy conversion terms from budget equations of EKE and Mean Available Potential Energy (MAPE) represented as:

$$\frac{\partial K_E}{\partial t} = C_k + C_{pk} - D_E + K_{EB} + \phi_{EB} \tag{6}$$

and

$$\frac{\partial A_E}{\partial t} = C_A - C_{pk} + G_E + A_{EB} \tag{7}$$

where K_E is the average eddy kinetic energy and A_E is the eddy available potential energy, C_k is barotropic energy conversion, C_{pk} is the baroclinic energy conversion term, and D_E is the frictional dissipation. The conversion term of zonal available potential energy to eddy available potential energy due to eddy heat flux along the zonal mean temperature gradient is given by C_A, and the generation of eddy available potential energy by diabatic heating is given by G_E. K_{EB} and A_{EB} are the boundary fluxes of eddy kinetic and available potential energy, respectively. ϕ_{EB} is the boundary pressure work performed by the eddies.

The energy conversion terms are calculated as

$$C_k = -\overline{\overrightarrow{V'_H}.(\overrightarrow{V'}.\nabla)\overrightarrow{V_H}} \tag{8}$$

$$C_{pk} = -\frac{R}{p}\overline{\omega' T'} \tag{9}$$

https://doi.org/10.5194/egusphere-2026-2879
Preprint. Discussion started: 11 June 2026

$$C_A = -\frac{c_p \gamma}{\overline{T}} \overline{\overrightarrow{V_H'} T'} . \nabla_H \overline{T} \tag{10}$$

$$G_E = \frac{\gamma}{\overline{T}} \overline{Q_1' T'} \tag{11}$$

where T is daily mean temperature, ω = dp/dt, is the vertical velocity, Q_1 is the apparent heat source, V_H is the horizontal wind speed, and p is pressure. Also, $\gamma = \frac{\Gamma_d}{\Gamma_d - \Gamma}$, where Γ_d and Γ are the dry adiabatic and observed lapse rates, respectively, c_p is the heat capacity at constant pressure, and R is the dry air gas constant.

The apparent heat source is calculated as:

$$Q_1 = \frac{c_p T}{\theta} \left(\frac{\partial \theta}{\partial t} + u \frac{\partial \theta}{\partial \phi} + v \frac{\partial \theta}{\partial \lambda} + \omega \frac{\partial \theta}{\partial p} \right) \tag{12}$$

where θ is the potential temperature.

The overbar denotes a temporal mean and primes in these equations are calculated as 3-5 day Butterworth bandpass filter applied to daily fields. The higher-order terms (triple products of perturbations) in equations 6 and 7 are omitted from the analysis (Hsieh and Cook, 2007).

4 Results

4.1 Model Validation

4.1.1 Representation of the mean state

To evaluate the performance of the IFS historical simulation, we begin by comparing its mean climatological fields against observations and reanalysis data. Figure 1a and 1b present the spatial distribution of 2-meter temperature and mean sea level pressure from both ERA5 and the IFS historical run in JJAS season. The presence of the Saharan Heat Low (SHL) is captured in both datasets. The IFS simulation reproduces the intensity and spatial extent of SHL with reasonable accuracy when compared to ERA5, although it exhibits a slight overestimation of temperature and a corresponding underestimation of sea level pressure at the SHL core. Additionally, over the tropical Atlantic, particularly in the cold tongue region, the IFS simulation shows moderately elevated ($\sim$ 2K) 2-meter temperatures relative to ERA5.

Figure 1c and 1d show the JJAS mean precipitation from MSWEP and the IFS historical simulation, respectively. The spatial distribution of the monsoon rainbelt is broadly consistent between the two figures, suggesting that the IFS model reasonably captures the large-scale monsoon precipitation pattern. However, the IFS simulation tends to overestimate precipitation over the marine Intertropical Convergence Zone (ITCZ) and regions of high orography, particularly over the Niger Basin and areas south of the Jos Plateau. Rainfall is also overestimated over the Guinea Gulf, off the coast of West Africa. Conversely, there is an underestimation of precipitation over the northern oceanic ITCZ, which affects the westernmost Sahel. These features could

https://doi.org/10.5194/egusphere-2026-2879
Preprint. Discussion started: 11 June 2026

be connected to the warm bias in 2-meter temperature in the cold-tongue region (Vizy and Cook, 2001, 2002). Also displayed in fig. 1c and 1d are the corresponding surface wind vectors, derived from ERA5 and the IFS historical run respectively. The model reproduces the surface wind patterns, especially the low-level monsoon flow with considerable accuracy.

Regarding the vertical cross-sections of omega and omega–meridional wind, the ERA5 reanalysis (Fig. 1e) reveals two distinct cells of vertical motion: a deeper cell located between approximately 2°N and 12°N, associated with moist convection over the monsoon rainbelt, and a shallower cell centered near 18°N, corresponding to dry convection over the SHL. The IFS historical simulation captures both convective cells with reasonable fidelity, as shown in Fig. 1f. The simulated locations of these features closely match those in ERA5. However, the IFS tends to overestimate the strength of monsoon-related vertical motion, with the simulated moist convection extending more deeply in the troposphere, reaching up to 200 hPa. This deeper convection in IFS could be related to the reduced cloud base mass flux setup used in this simulation, which enhances CAPE compared to the model with a fully active deep convection scheme (Becker et al., 2021; Takasuka et al., 2025). In contrast, the vertical motion associated with dry convection over the SHL in the IFS is of comparable magnitude to that in the reanalysis.

Figures 1g and 1h illustrate the JJAS mean wind speed at 600 hPa from ERA5 and the IFS historical simulation, respectively. This level is representative of the African Easterly Jet (AEJ), a prominent mid-tropospheric feature over West Africa. The AEJ is formed due to the strong thermal contrast between the hot Saharan landmass and the cooler equatorial Atlantic and is sustained by the juxtaposition of moist convection to the south and dry convection to the north (Nicholson, 2013). AEWs typically propagate along both flanks of the AEJ, with a greater frequency in the latitudinal zone south of the jet core. This region, situated between the axes of the AEJ and the upper-tropospheric Tropical Easterly Jet (TEJ), provides a favorable environment for wave development, although a fraction of AEWs also form along the northern flank of the AEJ (Thorncroft and Hoskins, 1994; Thorncroft and Blackburn, 1999). Compared to ERA5, the IFS historical simulation overestimates the intensity and zonal extent of the AEJ (Fig. 1h), which may have implications for the representation of AEW activity and downstream precipitation patterns in the model.

4.1.2 Representation of AEWs

To assess the model's representation of AEWs, we begin by comparing the mean wave characteristics of the IFS historical simulation with those from ERA5 reanalysis. Specifically, we examined the standard deviation of 3–5 day bandpass-filtered meridional wind at 700 hPa, precipitation, and Eddy Kinetic Energy (EKE) at 700 hPa during the JJAS season. Figures 2a and 2b show the standard deviation of 3–5 day filtered meridional wind at 700 hPa from ERA5 and the IFS simulation, respectively. In both datasets, the region of maximum variability is located around 20°N over the Atlantic, consistent with the climatological position of the AEJ and associated AEW activity. However, notable discrepancies exist between the model and reanalysis. In particular, the IFS simulation underestimates the variability in the equatorial Atlantic and overestimates it over the western Sahel region. Outside these areas, the variability of bandpass filtered meridional wind is comparable between ERA5 and the IFS simulation.

Figures 2c and 2d present the standard deviation of 3–5 day bandpass-filtered precipitation from MSWEP and the IFS historical simulation, respectively. Overall, the IFS simulation exhibits an overestimation of precipitation variability along the

https://doi.org/10.5194/egusphere-2026-2879
Preprint. Discussion started: 11 June 2026

AEW pathway. The most pronounced positive biases are found over the tropical Atlantic, centred around 8°N, as well as over the Sahel and regions of high orography. Interestingly, the model's overestimation in 3-5 day precipitation variability over land is not translated to the climatological mean, which showed no consistent bias over all of West Africa (Fig. 1c-d). These biases suggest that the model has enhanced convective responses associated with AEW activity in these regions.

Figures 2e and 2f show the distribution of Eddy Kinetic Energy (EKE) at 700 hPa for ERA5 and the IFS historical simulation, respectively. The spatial pattern of EKE closely resembles that of the filtered meridional wind variability, with maximum values located off the West African coast in ERA5. This EKE maximum is notably underestimated in the IFS simulation. More broadly, the IFS model consistently underestimates EKE compared to ERA5 across the region. As the meridional wind variability was not underestimated over the western Sahel and the tropical North Atlantic, it suggests an underestimation of the zonal wind variability related to AEWs. Interestingly, while the IFS simulation underrepresents the variability of bandpass-filtered EKE, it simultaneously overestimates the variability in precipitation, indicating potential inconsistencies in the model's representation of dynamical-convective coupling associated with AEWs.

To investigate the spatial structure of African Easterly Waves (AEWs), meridional wind anomalies at 700 hPa were extracted using a Butterworth bandpass filter to isolate 3–5 day waves. The 700 hPa level is commonly used for AEW identification and analysis (Carlson, 1969; Berry and Thorncroft, 2005, 2012; Kiladis et al., 2006). Composite anomalies of wind and precipitation were constructed following the methodology outlined in Section 3, using time lags of –4, –2, +2, and +4 days relative to the AEW trough passage. Figure 3a–e presents the composite evolution of AEW-associated circulation and precipitation anomalies from ERA5 and MSWEP, respectively. A well-defined wave structure is evident, with a wavelength of approximately 3000 km. The northern extent of the wave reaches into the Sahara, while precipitation anomalies are primarily concentrated in the southern part of the cells. Positive rainfall anomalies are located near the northerly flow ahead of the trough, whereas negative anomalies occur to the south of the ridge, in association with southerly winds. The strongest wind anomalies are found near 5°W, consistent with the location of the base point (1°W, 11.5°N), across all time steps. As the wave propagates westward into the Atlantic, it also shifts northward. The trough and ridge structures exhibit a northeastward tilt, consistent with wave characteristics observed in previous studies (e.g. Hsieh and Cook, 2007; McCrary et al., 2014; Raj et al., 2023).

Figures 3f–j illustrate the composite evolution of 3–5 day AEWs and the associated precipitation anomalies from the IFS historical simulation. The simulated AEWs exhibit a wavelength comparable to that observed in ERA5, indicating that the model captures the large-scale spatial scale of these disturbances reasonably well. At time lag -4 days, the model underestimates the density of streamlines (Fig. 3a and 3f), while the trough and ridge patterns in the simulated wind field are more distinctly defined just before and after lead time 0 (Fig. 3b-e and 3g-j), with streamlines appearing more tightly packed than in the reanalysis. Notably, over the Atlantic the differences beteewen IFS and ERA5 also changes with time lag, with weaker wind anomalies and less tight streamlines in the model before time lag 0 to a more pronounced westward propagation of AEWs at later lags in the IFS simulation, with the waves extending farther into the tropical Atlantic than in ERA5. This suggests stronger wave perturbations in the model but less recurrence than in the reanalysis, leading to a mean underestimation of EKE. The number of AEW days in the historical simulation is also underestimated in comparison with that in ERA5 (Table 1). The

https://doi.org/10.5194/egusphere-2026-2879
Preprint. Discussion started: 11 June 2026

northeastern tilt of the waves is also weaker in the IFS than in ERA5, which agrees with the underestimation in EKE in Fig.2e-f and not so much in the variability of the meridional wind component (Fig.2a-b).

Overall, the IFS simulation tends to overestimate the precipitation anomalies across all time lags when compared to the MSWEP dataset (Fig. 3), in agreement with the overestimation shown in Fig.2c-d. Despite this overestimation of precipitation anomalies, the relative positioning of positive and negative rainfall anomalies with respect to the AEW wave core is consistent with observations.

To further evaluate the model's representation of AEW-related rainfall, the total JJAS precipitation was decomposed into contributions from AEW and non-AEW days, following the methodology outlined in Section 3. While the IFS historical simulation reproduces the mean seasonal rainfall reasonably well compared to observations, this decomposition reveals notable differences in the underlying rainfall mechanisms.

Figures 4a–c display the difference between AEW and non-AEW rainfall for CHIRPS, MSWEP, and the IFS historical simulation, respectively. In the CHIRPS dataset (Fig. 4a), AEW events contribute substantially to rainfall over the Sahel and the Guinean coast, indicating their dominant role in modulating precipitation in these regions. A similar spatial pattern is evident in the MSWEP dataset (Fig. 4b), though some isolated areas over the equatorial Atlantic exhibit greater rainfall associated with non-AEW events. In contrast, the IFS historical simulation (Fig. 4c) shows a markedly different distribution. The model exhibits a pronounced dipole structure, with enhanced AEW-related rainfall concentrated in a zonally continuous band between 10°–15°N, encompassing the Sahel. South of this AEW-dominated rainbelt, the equatorial Atlantic displays a secondary rainbelt primarily associated with non-AEW events. Both features are more zonally continuous and intense in the model compared to observations and are statistically significant, suggesting a possible over-amplification of the AEW signal and its latitudinal separation from non-AEW precipitation within the IFS simulation, in agreement with previous analysis (Fig. 2c-d and 3). Figures 4d-f show the difference in the percentage of days with extreme rainfall —defined as daily precipitation exceeding the 95th percentile threshold— between AEW and non-AEW days, using CHIRPS, MSWEP, and the IFS historical simulation, respectively. The spatial distribution in CHIRPS (fig. 4d) shows that across much of the Sahel and the Guinea Coast, AEW days are associated with a greater frequency of extreme rainfall, supporting the role of AEWs in modulating extreme precipitation events (Crétat et al., 2015). Over the Sahel up to approximately 15ºN the values with strongest positive rainfall mean differences between AEW and non-AEW days (fig. 4a) tend to coincide with those where the strongest positive differences in extreme occurrence are shown (fig. 4d), forming a band between 8 and 10ºN close to the one where EKE maximum values are shown (fig. 2e). Some isolated blue patches in the equatorial regions suggest localized zones where non-AEW events also contribute significantly to extremes, and tend to agree with negative values of rainfall difference between AEW and non-AEW days (fig. 4a). The spatial pattern in MSWEP (fig. 4e) generally agrees with that in CHIRPS, showing a broad zone of positive anomalies across the Sahel and Guinea Coast, highlighting the significant contribution of AEWs to the occurrence of heavy rainfall events in these regions and their influence in the mean rainfall difference (fig. 4b). However, compared to CHIRPS, MSWEP shows a more granular structure, particularly in the southern part of the domain. Notably, several regions across the equatorial belt —including the Gulf of Guinea and parts of Central Africa— display negative values, suggesting that non-AEW-related convection contributes more frequently to extremes in these areas. This spatial distribution

https://doi.org/10.5194/egusphere-2026-2879
Preprint. Discussion started: 11 June 2026

implies that while AEWs are a major driver of extreme rainfall across the northern tropical belt, other non-AEW mechanisms may dominate rainfall extremes farther south. IFS historical simulation (fig. 4f) reveals a similar broad spatial structure, with an enhanced occurrence of extreme rainfall on AEW days within a latitudinal band centered around 10°–15°N. However, the magnitude and zonal continuity of this signal are stronger and more spatially coherent than in CHIRPS and MSWEP, particularly over West Africa. This suggests that while the IFS model captures the link between AEWs and extreme rainfall, it overestimates the spatial extent and intensity of this relationship. Additionally, the presence of negative values to the south of this AEW-influenced rainbelt, especially over the equatorial Atlantic, indicates overestimation of extremes related to non-AEW events in that region.

Figures 4g–i exhibit the difference in the percentage of days with moderate rainfall, defined as days with precipitation below the 75th percentile, between AEW and non-AEW days, using the CHIRPS, MSWEP, and IFS historical simulation, respectively. In CHIRPS data (fig. 4g), positive values generally prevail over land, except for patches of negative values that tend to overlay the band between 8 and 10ºN where the extreme events were more strongly connected to AEW days (fig. 4d). This suggests that over land, AEWs tend to promote more rainfall extremeness across their core region of passage and more moderate events in the margins to the north and south of this core area. The combination of both provides more rainfall over most land regions related to AEW (fig. 4a). MSWEP (fig. 4h) shows a more spatially variable and noisy distribution. However, negative AEW vs non-AEW differences in moderate rainfall also tend to appear where maximum positive differences in extreme rainfall are located (fig. 4e), while AEW days promote moderate rainfall to the margins, more clearly to the north of 15ºN, in general agreement with CHIRPS. A strong and coherent pattern, with a band of positive anomalies centered over 10°–15°N over the Atlantic and western Sahel and east of 10ºE and negative anomalies across the equatorial Atlantic, the central Sahel (10ºW-10ºE) and Central Africa is observed in IFS historical simulation (fig. 4i). Combined with the difference in extremes (fig. 4f), it suggests that AEWs in the model are strongly associated with an increase of all types of rainfall events in the eastern Sahel, eastern Africa and the Atlantic between 10ºN and 15ºN, a decrease in the frequency of occurrence in all types of event in the Atlantic south of 8ºN, and a shift of rainfall events towards more extremeness over land in the central Sahel, Gulf of Guinea and central Africa. Compared to observations, the IFS simulation tends to amplify the meridional separation between AEW and non-AEW moderate rainfall zones (fig. 4i), consistent with results seen in the extreme rainfall analysis (fig. 4f). As in the observations, the pattern of rainfall differences (fig. 4c) tends to be dominated by that coming from the differences in extremes (fig. 4f).

Overall, these figures suggest that AEWs play a key role not only in producing extreme rainfall, especially close to the AEW core, but also in modulating moderate precipitation, particularly to the north of this core. However, the IFS model exhibits a strong dipole pattern in precipitation dominated by the extreme events, suggesting a much stronger role of AEW in promoting convection in the model.

To evaluate the robustness of the future AEW projections, we first assess how well the IFS model simulates AEW energetics during the historical period. Figure 5 presents the meridional height cross-sections of the four key energy terms —baroclinic conversion (C_{pk}), barotropic conversion (C_k), diabatic generation of eddy available potential energy (G_E), and conversion from zonal mean to eddy potential energy (C_A)— for 3–5-day AEWs, as derived from both ERA5 reanalysis and the IFS historical

https://doi.org/10.5194/egusphere-2026-2879
Preprint. Discussion started: 11 June 2026

simulation. The IFS model captures the spatial structure and vertical distribution of baroclinic conversion (C_{pk}) reasonably well, with two regions of positive conversion (e.g. generation of eddy kinetic energy) in the upper and lower troposphere and a negative area (e.g. destruction of eddy kinetic energy) at 700 hPa (Fig. 5a-b), in agreement with previous studies (e.g. Hsieh and Cook, 2007; McCrary et al., 2014). In both IFS and ERA5, C_{pk} in the mid-to-upper troposphere shows positive values between 10°N and 15°N with a core around 400–300 hPa, indicating strong vertical overturning and energy conversion due to convective heating. However, the IFS simulation overestimates the magnitude of C_{pk} in the upper troposphere compared to ERA5. Though we cannot rule out ERA5 could be underestimating this term due to the underlying, fully active convection scheme used by the reanalysis, the hypothesis of an overestimation in the IFS, attributed to amplified latent heating from more active convection, is in accordance with the previous results of too strong precipitation variability associated with AEWs in the model (Figs. 2d and 3), and too much precipitation, especially extreme events, in AEW compared to non-AEW days with respect to observations (Fig. 4), which could be contributing to the overall too strong convection in IFS (Fig. 1f).

The meridional profile of barotropic conversion (C_k) shows a center of positive values south of the AEJ core just above ~700 hPa, concentrated between 6°N and 14°N. IFS reproduces this structure but exhibits more limited and less intense values compared to ERA5, suggesting a smaller equatorward transport of easterly momentum associated to AEWs than in observations - which could be connected to the less tilted structure of the waves in the model (Fig. 3) - and/or a weaker horizontal wind shear in the simulated AEJ, potentially linked to biases in the simulated meridional temperature gradient that drive the jet.

The diabatic generation term (G_E) shows an upper-tropospheric maximum near 300 hPa in both datasets, aligned with regions of positive C_{pk}. This confirms the role of latent heat release in generating eddy available potential energy and sustaining baroclinic growth. IFS simulates a stronger G_E magnitude than ERA5, again reflecting more vigorous convection associated with AEWs. This tight spatial coupling between G_E and C_{pk} highlights the importance of convectively driven baroclinic amplification in AEW maintenance. The C_A term, which represents the conversion from zonal mean to eddy potential energy via meridional heat fluxes, is also well represented in the IFS simulation. Both ERA5 and IFS show a positive band of C_A between 16°N and 22°N, although the IFS extends this region equatorward and overestimates its intensity. This may suggest a broader region of eddy generation in the model due to enhanced thermal gradients and eddy activity.

Overall, the IFS model successfully captures the key energetic features of 3-5-day AEWs when compared to ERA5. While the model shows overestimation in the magnitude of terms related to deep convection (G_E and C_{pk} at around 300 hPa and 10ºN), the spatial structure and vertical placement are consistent with reanalysis. These biases are within the expected range for convection-permitting GCMs and likely reflect differences in convective treatment and moist processes. Note that we have assessed biases by comparing to ERA5 estimates, which might be affected by the use of a fully active convection scheme, especially over regions and variables not well constrained by observations. In any case, the close agreement between IFS and ERA5 provides confidence in the model's ability to simulate AEW dynamics and energetics, thereby justifying its use in future projection studies.

https://doi.org/10.5194/egusphere-2026-2879
Preprint. Discussion started: 11 June 2026

4.2 Future Projection

Figure 6a shows the difference in near-surface air temperature at 2 meters during JJAS, between the IFS future and historical simulations. The map shows widespread warming across West Africa, with the most intense warming—exceeding 2°C—concentrated over the northern Sahara, extending northeastward into Egypt. Warming is generally stronger over land than over adjacent ocean regions and the gradient of warming increases northward, reflecting both the reduction in cloud cover and enhanced surface radiative heating in drier regions. Areas of statistical significance are indicated by stippling and cover much of the region, suggesting that the projected warming signal is robust.

Figure 6b displays the projected change in mean JJAS precipitation, calculated as the difference between the IFS future and historical simulations. There is a widespread increase in precipitation over West Africa, with regions of strong increase occurring over parts of the central and eastern Sahel, the Gulf of Guinea region, and the southern branch of the Atlantic ITCZ, where precipitation changes by more than 1.5 mm/day. This wetting is statistically significant in several areas, as indicated by stippling, suggesting a robust model signal. In contrast, precipitation decreases off the coast of the Gulf of Guinea and particularly over westernmost West Africa and the northern part of the Atlantic ITCZ, suggesting a slight southward shift of the marine ITCZ affecting the West African coast. The west-east dipole pattern in the mean precipitation over the Sahel as a response to climate change is consistent with the mean projected changes from coarser grid models (e.g. Monerie et al., 2020; Biasutti, 2013) and in line with observed long-term trends contrasting changes in the east and west Sahel in mean precipitation and the occurrence of extremes events (Lebel and Ali, 2009; Panthou et al., 2018; Blanchet et al., 2018).

As the analysis of changes in the precipitation regime suggests two separate regions with different responses, the cross-sections for omega are averaged over ocean regions (Fig. 6c) and land regions (Fig. 6d) within West Africa. The oceanic cross-section (Fig. 6c) reveals a dipole structure in omega anomalies, with enhanced convection to the south of the climatological location of main ascent reaching up to the upper troposphere (200 hPa) and increased subsidence between 6°–11°N reaching the mid-upper troposphere (up to 300 hPa). This pattern suggests a southward shift of the oceanic ascent region, consistent with the rainfall response. Over land (Fig. 6d), the model projects a strong and vertically extensive increase in ascent across the Sahel, particularly around 6°–14°N, with compensating subsidence on either side of the main updraft zone. A similar intensification of convection is also seen over the equator. This indicates an intensification and vertical deepening of convective activity over land in the future climate, consistent with the local rainfall response. The stippling in both panels denotes areas of statistical significance, highlighting regions where the projected changes in omega are robust. Together, these figures underscore a substantial reorganization of the tropical circulation system under climate change, with implications for rainfall distribution and convective activity.

Figure 6e shows the projected change in JJAS mean wind speed at 600 hPa between the IFS future and historical simulations. This level corresponds to the core of the AEJ as in fig. 1h. The spatial distribution of wind speed differences reveals a no significant changes to the AEJ core. In contrast, isolated regions in the western Sahara and along the Atlantic coast exhibit patches of increased wind speed. A similar significant increase in wind speed is seen over Atlantic centred around 12ºN and over eastern Sahel.

https://doi.org/10.5194/egusphere-2026-2879
Preprint. Discussion started: 11 June 2026

Figure 7 shows the difference in 3–5 day bandpass-filtered eddy kinetic energy (EKE) at 700 hPa between the IFS future and historical simulations for the JJAS season, representing projected changes in AEW activity. The figure reveals a strong dipole structure. Over West Africa and the Guinea Gulf, EKE increases significantly in the future simulation, with anomalies exceeding 0.5 m^2/s^2 close to the region of strongest climatological EKE (Fig. 2f). This indicates a significant intensification of AEW activity over West Africa. In contrast, a large region over the north tropical Atlantic (north of 10°N and between 30°–60°W) exhibits decreased EKE, with anomalies dropping below –0.5 m^2/s^2. This suggests a weakening of AEW activity over the Atlantic, potentially linked to the weakening of Atlantic hurricane activity. This dipole pattern implies a spatial reorganization of AEW activity under future climate conditions, with increased wave amplitude or frequency over land and reduced activity over the ocean. The weakening of the AEW footprint on the tropical Atlantic is also seen when comparing the 700 hPa waves shown in Fig. 3: after the passage over land of the main wave (lag times $\geq$0), stream lines around the point 35ºW, 18ºN tend to be less tight in the projection run (Fig. 3m-o) than in the historical one (Fig. 3h-j). Interestingly, at negative lag times, the concentration of streamlines suggests higher overall activity in the projection run (Fig. 3k-l) than in the historical run (Fig. 3f-g). This could be related to the overall increase in the number of AEWs detected: the ratio of AEW to total number of days increases from 44% to 55% from the historical to the projection run (Table 1).

Figure 8 presents the projected changes in the four energetics terms associated with 3–5-day African Easterly Waves (AEWs), computed as the anomaly between the projection and the historical IFS simulations. These terms include baroclinic conversion (C_{pk}), barotropic conversion (C_k), diabatic generation of eddy available potential energy (G_E), and conversion from zonal mean to eddy potential energy (C_A). Together, they describe the dynamical and thermodynamical processes maintaining AEWs and how these are influenced by climate warming. The baroclinic conversion term (C_{pk}) exhibits an amplification of the climatological values, especially in the upper troposphere above 500 hPa between 6°N and 15°N. This positive anomaly suggests enhanced conversion of eddy available potential energy into eddy kinetic energy, likely driven by intensified latent heating and stronger vertical overturning. The deepened vertical extent of the anomaly indicates more vigorous convective coupling, consistent with previous studies (e.g. Raj et al., 2023; Akinsanola et al., 2025), where baroclinic amplification was linked to moist convection.

Barotropic conversion (C_k) shows a positive anomaly south of the AEJ core, implying an intensification of the climatological production of EKE associated with the AEJ. This pattern could be related to the increased horizontal shear in the eastern part of the domain (Fig. 6e) and a more unstable AEJ with more equatorward transport of easterly momentum, promoting greater energy transfer from the mean flow to the waves. Such a response is typically associated with enhanced meridional thermal gradients in a warmer climate (Akinsanola et al., 2025), which strengthen the AEJ and support wave growth via barotropic mechanisms.

The G_E field shows strong positive anomalies co-located with the C_{pk} anomalies in the upper troposphere, underscoring the role of enhanced diabatic heating in generating eddy available potential energy. This further reinforces the coupling between latent heating and baroclinic processes. The alignment between G_E and C_{pk} suggests a more efficient energy conversion loop in the future climate, driven by intensified convective heating.

https://doi.org/10.5194/egusphere-2026-2879
Preprint. Discussion started: 11 June 2026

Finally, the C_A anomalies show an intensification of the meridional thermal advection related to the Saharan heat low, which enhances the conversion of zonal mean to eddy available potential energy. It could be related to enhanced southward eddy heat fluxes and increased low-level thermal gradient (Fig. 6a), which are common features in CMIP-type projections of West African monsoon dynamics (Akinsanola et al., 2025), but it is different from the southward shift suggested by higher resolution AGCMs (Raj et al., 2023).

In summary, the IFS simulations project a thermodynamically and dynamically consistent intensification of 3–5-day AEW energetics over land under near-term SSP3-7.0 forcing. Enhanced latent heat release drives stronger diabatic generation and baroclinic conversion, while increased AEJ shear supports barotropic energy transfer. The increased low-level thermal gradient provides further eddy generation related to the Saharan heat low. These results collectively highlight a robust future intensification of AEW activity over land and are in line with the mechanisms identified in Raj et al. (2023) and Akinsanola et al. (2025).

We now focus on further investigating changes in the mean JJAS precipitation shown in Fig. 6a through their relation with changes in AEWs. As it was shown before, there is an increase in the number and strength of AEWs over land. The stronger AEWs in the projection tend to be accompanied by stronger precipitation anomalies, as it can be seen when comparing fig. 3f-h with fig. 3k-o. In addition, the increase in the number AEW days in the projection is expected to promote more precipitation over the Sahel, as AEW days in the model are associated with more precipitation than non-AEW days there and less over the Atlantic south of 7ºN (Fig. 4c). However, non-AEW could also be associated with changes in rainfall. To evaluate the relevance of these potential factors, we decompose the change in mean JJAS precipitation into three contributing components using the analytical framework described in Section 3, based on Equation 4. In this equation, the total projected change in precipitation is expressed as the sum of three terms:

1. the contribution from changes in mean precipitation coming from both AEW and non-AEW days,
2. the contribution from changes in the number of AEW days, and
3. a cross-product term

Figure 9a shows the addition of the three separate terms and reproduces the total change in precipitation between the IFS future projection and the historical simulation (Fig. 6b). The contribution from the cross-product term is negligible (fig. 9d), while that coming from the increase in AEW days shows, as expected, a meridional dipole of rainfall promoting more precipitation over the Sahel in the projection (fig. 9c). However, the main change in mean JJAS precipitation comes from the changes in the magnitude of precipitation occurring in both subsets, AEW and non-AEW days (fig. 9b). This latter term sets the pattern of change and is only weakly affected by the enhancement in the share of AEW days in the projection that further increases precipitation over central Sahel and moderates the drying over westernmost Sahel.

In addition, in figure 10 we show projected changes in mean precipitation during AEW days (ΔP_A, fig. 10a) and during non-AEW days (ΔP_N, fig. 10b). Though there are local differences, both patterns resemble the mean change displayed in fig. 6a, showing a southward shift of the Atlantic ITCZ, widespread increases in rainfall over West Africa, with particular regions

https://doi.org/10.5194/egusphere-2026-2879
Preprint. Discussion started: 11 June 2026

of strong increase in the central and eastern Sahel and a drying over the westernmost Sahel and small patches off the coast in the Gulf of Guinea. These results suggest that the projected changes in precipitation cannot be solely connected to the stronger and more frequent AEW activity. As non-AEW days show a similar change of precipitation, it suggests other dynamical and thermodynamical changes in the monsoon affecting similarly rainfall over AEW and non-AEW days are at the root of mean precipitation changes.

To assess the projected changes in rainfall characteristics in future climate scenarios, fig. 11 exhibits the differences in the percentage of extreme rainfall days (above the 95th percentile of rainy days), moderate rainfall days (below the 75th percentile), and rainy days between the IFS future and historical simulations for the JJAS season. The analysis is further separated into AEW days and non-AEW days. Panels 11a and 11b show the projected changes in the frequency of extreme rainfall days for AEW and non-AEW conditions, respectively. Across much of West Africa, particularly over the Sahel and Guinea Coast, both AEW and non-AEW days exhibit an increase in the frequency of extreme rainfall events. Although this increase is more pronounced on AEW days (Fig. 11a), it is noteworthy that non-AEW also substantially contribute to changes in extreme event occurrences in the future climate. A similar decomposition to the one used for the mean JJAS rainfall also shows that the contribution due to the increase in the number of AEW days is of second-order importance to explaining the overall change in extremeness (not shown).

Panels 11c and 11d illustrate the projected changes in the percentage of moderate rainy days under AEW and non-AEW conditions. In contrast to the changes in extreme rainfall days, there is a substantial decrease in the percentage of moderate rainfall days, especially across Central West Africa and the western Sahel, with the strongest reduction observed on non-AEW days (Fig. 11d). This indicates a future shift toward less frequent moderate precipitation events in these regions. A notable difference between AEW and non-AEW changes is the reduction in moderate events over the eastern Atlantic at about 10ºN and 20ºW shown during non-AEW, which is transformed into an increase for AEW days. On the other hand, an increase in the percentage of moderate rainfall days is observed over the equatorial Atlantic, southern Sahara, and east Africa during both AEW and non-AEW days. The total changes in the occurrence of AEW and non-AEW rainy days are shown in figs. 11e and f, respectively. The model projects a similar pattern to that in the change in the percentage of moderate rainfall days. The substantial decrease in AEW and non-AEW rainy days over the west and south-central Sahel, despite the increase in the frequency of extremes, suggests that the contribution to total change in rainfall there (fig. 6b) comes mostly from extreme events. Conversely, over the southern Sahara, rainfall increase is mostly related to an enhancement of rainy days, especially of moderate events. Noteworthy is the precipitation decrease in the westernmost Sahel, which is mainly linked to a reduction in extreme events for AEW days and to moderate events for non-AEW days.

Overall, Figure 11 demonstrates a general shift in the rainfall regime over Sahel under future climate conditions, characterized by: an increase in the frequency of extreme rainfall events, slightly more pronounced on AEW days than non-AEW days, a decrease in the frequency of moderate rainfall events, primarily associated with non-AEW conditions over the western Sahel and a similar decrease in the percentage of rainy days.

https://doi.org/10.5194/egusphere-2026-2879
Preprint. Discussion started: 11 June 2026

4.3 Mechanisms Contributing to Future Changes in AEW Activity

The projected changes in AEW activity under future climate scenarios raise the question about the underlying mechanisms responsible for these changes. As discussed in the introduction, several theories have been proposed to explain the genesis and amplification of AEWs, which focuses on the dynamical and thermodynamical environment that supports their development. One of the key dynamical features essential for AEW growth is the reversal of the meridional potential vorticity (PV) gradient, a mechanism that facilitates the necessary barotropic and baroclinic instability for wave amplification (Thorncroft and Blackburn, 1999; Dickinson and Molinari, 2000; Diaz and Aiyyer, 2013). This gradient reversal results from the combined effects of PV destruction by dry convection over the Sahara and PV generation by deep, moist convection associated with the Intertropical Convergence Zone (ITCZ), typically centered near 10°N (Diaz and Aiyyer, 2013). Southern-track AEWs, in particular, are known to form through the interaction of positive and negative meridional PV gradients at mid-levels, and are often found along or south of the zonally elongated PV maximum (Pytharoulis and Thorncroft, 1999; Diaz and Aiyyer, 2013).

To investigate how these features evolve in the future climate, we examined the change in PV at 700 hPa between the IFS historical simulation and the future projection for the JJAS season. Figure 12a illustrates the difference in PV between the two periods, highlighting a pronounced increase in the PV inversion band centered around 10°N. This enhancement of the PV gradient in the future scenario could play a significant role in supporting the projected increase in both the frequency and intensity of AEWs.

To further understand the drivers of this PV enhancement, we analyzed the future changes in relative vorticity and the vertical gradient of potential temperature $(\partial\theta/\partial p)$, which are key contributors to PV generation as PV is defined as $PV = -g(\partial\theta/\partial p)(\zeta + f)$ where ζ is the relative vorticity, f is the Coriolis parameter, and g is the acceleration due to gravity (Figs. 12b and 12c). Our results indicate that while relative vorticity exhibits little change across the region, there is a significant reduction in $\partial\theta/\partial p$. This reduction reflects an increase in static stability, which is consistent with results from previous studies about warming climate in the tropical regions, where moist convection tends to maintain the vertical lapse rate close to the moist adiabatic lapse rate which, in turn, decreases with temperature making the atmosphere more statically stable (Knutson and Manabe, 1995). The observed change in static stability contributes to the strengthening of the PV inversion and may partly explain the projected increase in AEW activity.

In addition to the internal dynamics associated with PV gradients and static stability, AEW genesis is also strongly influenced by the upstream atmospheric conditions over East Africa, where orographic features and convective processes play a critical role in generating precursor disturbances. Previous studies highlight the importance of the Ethiopian Highlands and East African topography in initiating AEWs through convectively generated disturbances (Hamilton et al., 2020; Hill and Lin, 2003). Orographic forcing, combined with strong diurnal convection in these regions, promotes latent heating and the generation of potential vorticity (PV) anomalies (Thorncroft et al., 2008; Fischer et al., 2024), which are subsequently advected westward and embedded within the AEJ, where they amplify through barotropic and baroclinic instability processes (White et al., 2021).

To assess whether upstream convective activity may contribute to the future changes in AEW characteristics, we analyzed the projected changes in variability of convection over East Africa, using outgoing longwave radiation (OLR) as a proxy for

https://doi.org/10.5194/egusphere-2026-2879
Preprint. Discussion started: 11 June 2026

deep convection. A 2.5–8 day bandpass filter was applied to daily OLR data for the JJAS season, and the standard deviation of this filtered signal was computed for both the historical and future IFS simulations. Figure 12d shows the difference in the standard deviation of OLR between the two the simulations, revealing a substantial increase in convective variability over East Africa in the future scenario. This enhancement of upstream convection could serve as an additional factor contributing to the increased frequency and intensity of AEWs by providing more frequent or stronger seeding disturbances.

In summary, the decomposition of PV changes, assessment of static stability, and evaluation of upstream convective variability together suggest that the projected intensification of AEW activity under future climate scenario may be driven by a combination of enhanced PV gradient inversion, increased atmospheric stability, and strengthened upstream convective forcing. These findings highlight the complex interplay between thermodynamic structure, wave dynamics, and upstream environmental conditions in modulating AEW behavior in a warming climate.

5 Discussion and conclusions

This study aims to provide a comprehensive assessment of projected changes in AEWs under the future climate scenario SSP3-7.0 using km-scale IFS simulations. The first part of the study evaluates the ability of IFS to represent AEWs by analysing the IFS historical simulation, the second part analyses the changes in AEW characteristics in the IFS future projection, and the third part investigates the mechanisms contributing to these changes.

The IFS historical simulation captures the broad spatial structure and energetics of AEWs with reasonable accuracy, including the wave variability and associated precipitation patterns. However, the model exhibits a consistent overestimation of precipitation variability and AEJ intensity, while underestimating the eddy kinetic energy (EKE) when compared to reanalysis and observational datasets. These biases reflect challenges common to high-resolution coupled models, but the performance of the model is substantially superior to previous studies (Akinsanola et al., 2025; Raj et al., 2023).

Future projections under the SSP3-7.0 scenario indicate a robust intensification of AEW activity over land, particularly over the western Sahel, with a concurrent weakening over the Atlantic sector. This spatial reorganization is accompanied by significant changes in the underlying energetics, including enhanced barotropic and baroclinic energy conversions and stronger diabatic generation of eddy available potential energy. This finding aligns with previous studies (e.g. Raj et al., 2023) that emphasize the role of latent heating and convective processes in modulating wave energetics under warming scenarios.

However, our results suggest that, though future warming will be accompanied by increased wave-related rainfall intensity and variability, the projected changes in mean JJAS rainfall over the central and eastern Sahel are not solely due to increased AEW activity. The higher number of projected AEW days promote more rainfall over the Sahel, but changes in rainfall during both AEW days and non-AEW days show a similar pattern and shape the overall observed JJAS rainfall change in West Africa and adjacent regions. The analysis of extreme and moderate rainfall events further confirms a that over the Sahel we can expect a near-future shift toward more frequent extreme rainfall days, alongside a reduction in moderate rainfall days and overall rainy day frequency.

https://doi.org/10.5194/egusphere-2026-2879
Preprint. Discussion started: 11 June 2026

The intensification of AEW activity in the future climate appears to be supported by multiple reinforcing mechanisms. An important contributor is the enhancement of the meridional potential vorticity (PV) gradient inversion around 10°N, which is a necessary condition for wave amplification through barotropic and baroclinic instability (Thorncroft and Blackburn, 1999; Diaz and Aiyyer, 2013). Our decomposition of PV changes suggests that the increase in static stability — resulting from climate warming in tropical regions where moist convection keep the temperature lapse rate close to the moist adiabatic rate (Knutson and Manabe, 1995) — plays a critical role in strengthening this inversion.

In addition, changes in upstream convective activity over East Africa emerge as a secondary driver. The projected increase in convective variability, as indicated by enhanced outgoing longwave radiation (OLR) variability, suggests more active wave seeding conditions over the Ethiopian Highlands and surrounding terrain. This supports the notion that upstream disturbances, amplified by orographic forcing and diurnal convection, may contribute to the increased frequency and intensity of AEWs in the future.

The projected intensification of AEWs under warming scenarios has critical implications for regional rainfall variability, extreme weather events, and agricultural resilience across West Africa. The shift toward more frequent and intense AEW-related precipitation could exacerbate flood risks in the Sahel and adjacent regions, even as the total number of rainy days decreases. These changes underline the importance of improving AEW representation in climate models to enhance seasonal forecasting, early warning systems, and adaptation strategies in the region.

The spatial reorganization of AEW energetics—particularly the land-based intensification and oceanic weakening—may also influence tropical cyclone formation potential in the Atlantic basin. Previous research suggests that the Atlantic AEW corridor plays a key role in seeding tropical cyclogenesis, and changes in wave activity may alter the statistics of hurricane development (Bercos-Hickey and Patricola, 2021; Skinner and Diffenbaugh, 2014). According to Núñez Ocasio et al. (2024), in a too moist environment, the phasing between the vorticity of AEW and the convection is less optimal. As a consequence, despite more convection due to the more humid environment, there is an effective decoupling between AEW and convection, resulting in less cyclogenesis once the AEW reaches the ocean. This could provide a potential explanation linking the occurrence of more moderate rainfall events during AEW-days over the eastern Atlantic off the West African coast and weaker EKE values downstream in the more moist future simulation.

Future research should explore the sensitivity of these projections to emission pathways (e.g., SSP scenarios), convective parameterizations, and coupling between ocean and atmosphere. Additionally, further analysis of AEW–tropical cyclone interactions and their role in modulating Atlantic hurricane activity under climate change remains an important area for investigation.

Author contributions. EM and JR designed the analysis. JR performed the analysis and led the writing, which was completed by EM. BF and TL discussed the results. TR and TB performed the simulations. All co-authors discussed and contributed to the final document

https://doi.org/10.5194/egusphere-2026-2879
Preprint. Discussion started: 11 June 2026

Competing interests. The authors declare no competing interests are present

Acknowledgements. This work was supported by the EU Horizon 2020 nextGEMS project (grant agreement 101003470). It used supercomputing resources of the German Climate Computing Centre (Deutsches Klimarechen-zentrum, DKRZ) under project ID 1153. We want to thank DKRZ staff for their continued support and the nextGEMS hackathon community for discussion and exchange of ideas and code. AI-assisted language tools were used to improve the clarity and readability of the manuscript text; all scientific content, analysis, and conclusions are solely the responsibility of the authors.

https://doi.org/10.5194/egusphere-2026-2879
Preprint. Discussion started: 11 June 2026

References

Akinsanola, A. A., Adebiyi, A. A., Bobde, V., Adeyeri, O. E., Tamoffo, A. T., and Danso, D. K.: Projected changes in African easterly wave activity due to climate change, Communications Earth & Environment, 6, 2, 2025.

Beck, H. E., Wood, E. F., Pan, M., Fisher, C. K., Miralles, D. G., Van Dijk, A. I., McVicar, T. R., and Adler, R. F.: MSWEP V2 global 3-hourly 0.1 precipitation: methodology and quantitative assessment, Bulletin of the American Meteorological Society, 100, 473–500, 2019.

Becker, T., Bechtold, P., and Sandu, I.: Characteristics of convective precipitation over tropical Africa in storm-resolving global simulations, Quarterly Journal of the Royal Meteorological Society, 147, 4388–4407, 2021.

Bercos-Hickey, E. and Patricola, C. M.: Anthropogenic influences on the African easterly jet–African easterly wave system, Climate Dynamics, 57, 2779–2792, 2021.

Bercos-Hickey, E. and Patricola, C. M.: Characteristics and trends of Atlantic tropical cyclones that do and do not develop from African easterly waves, Quarterly Journal of the Royal Meteorological Society, 150, 4951–4968, 2024.

Bercos-Hickey, E., Patricola, C. M., Loring, B., and Collins, W. D.: The relationship between African easterly waves and tropical cyclones in historical and future climates in the HighResMIP-PRIMAVERA simulations, Journal of Geophysical Research: Atmospheres, 128, e2022JD037 471, 2023.

Berry, G. J. and Thorncroft, C.: Case study of an intense African easterly wave, Monthly Weather Review, 133, 752–766, 2005.

Berry, G. J. and Thorncroft, C. D.: African easterly wave dynamics in a mesoscale numerical model: The upscale role of convection, Journal of the Atmospheric Sciences, 69, 1267–1283, 2012.

Biasutti, M.: Forced Sahel rainfall trends in the CMIP5 archive, Journal of Geophysical Research: Atmospheres, 118, 1613–1623, 2013.

Blanchet, J., Aly, C., Vischel, T., Panthou, G., Sané, Y., and Diop Kane, M.: Trend in the Co-occurrence of extreme daily rainfall in west africa since 1950, Journal of Geophysical Research: Atmospheres, 123, 1536–1551, 2018.

Brannan, A. L. and Martin, E. R.: Future characteristics of African easterly wave tracks, Climate Dynamics, 52, 5567–5584, 2019.

Carlson, T. N.: Synoptic histories of three African disturbances that developed into Atlantic hurricanes, Monthly Weather Review, 97, 256–276, 1969.

Crétat, J., Vizy, E. K., and Cook, K. H.: The relationship between African easterly waves and daily rainfall over West Africa: observations and regional climate simulations, Climate Dynamics, 44, 385–404, 2015.

Diaz, M. and Aiyyer, A.: The genesis of African easterly waves by upstream development, Journal of the Atmospheric Sciences, 70, 3492–3512, 2013.

Dickinson, M. and Molinari, J.: Climatology of sign reversals of the meridional potential vorticity gradient over Africa and Australia, Monthly weather review, 128, 3890–3900, 2000.

Dieng, A. L., Sall, S. M., Eymard, L., Leduc-Leballeur, M., and Lazar, A.: Trains of African easterly waves and their relationship to tropical cyclone genesis in the eastern Atlantic, Monthly Weather Review, 145, 599–616, 2017.

Elless, T. J. and Torn, R. D.: African easterly wave forecast verification and its relation to convective errors within the ECMWF ensemble prediction system, Weather and Forecasting, 33, 461–477, 2018.

Fink, A. H. and Reiner, A.: Spatiotemporal variability of the relation between African easterly waves and West African squall lines in 1998 and 1999, Journal of Geophysical Research: Atmospheres, 108, 2003.

https://doi.org/10.5194/egusphere-2026-2879
Preprint. Discussion started: 11 June 2026

Fischer, E. M. et al.: Diabatic Processes and Potential Vorticity Generation in Convective Systems, Geoscientific Model Development, 17, 4213–4235, https://doi.org/10.5194/gmd-17-4213-2024, 2024.

Funk, C., Peterson, P., Landsfeld, M., Pedreros, D., Verdin, J., Shukla, S., Husak, G., Rowland, J., Harrison, L., Hoell, A., et al.: The climate hazards infrared precipitation with stations—a new environmental record for monitoring extremes, Scientific data, 2, 1–21, 2015.

Hamilton, K. et al.: Topographic Influence on the African Easterly Jet and African Easterly Wave Energetics, Journal of Geophysical Research: Atmospheres, 125, e2019JD031 180, https://doi.org/10.1029/2019JD031180, 2020.

Hannah, W. M. and Aiyyer, A.: Reduced African easterly wave activity with quadrupled CO 2 in the superparameterized CESM, Journal of Climate, 30, 8253–8274, 2017.

Hersbach, H., Bell, B., Berrisford, P., Hirahara, S., Horányi, A., Muñoz-Sabater, J., Nicolas, J., Peubey, C., Radu, R., Schepers, D., et al.: The ERA5 global reanalysis, Quarterly journal of the royal meteorological society, 146, 1999–2049, 2020.

Hill, C. M. and Lin, Y.-L.: Initiation of African Easterly Waves in a Mesoscale Model: The Role of Convection, Journal of the Atmospheric Sciences, 60, 392–413, https://doi.org/10.1175/1520-0469(2003)060<0392:IOAEWI>2.0.CO;2, 2003.

Hsieh, J.-S. and Cook, K. H.: A study of the energetics of African easterly waves using a regional climate model, Journal of the Atmospheric Sciences, 64, 421–440, 2007.

Janiga, M. A. and Thorncroft, C. D.: Convection over tropical Africa and the east Atlantic during the West African monsoon: Regional and diurnal variability, Journal of Climate, 27, 4159–4188, 2014.

Kebe, I., Diallo, I., Sylla, M. B., De Sales, F., and Diedhiou, A.: Late 21st century projected changes in the relationship between precipitation, African easterly jet, and African easterly waves, Atmosphere, 11, 353, 2020.

Kiladis, G. N., Thorncroft, C. D., and Hall, N. M.: Three-dimensional structure and dynamics of African easterly waves. Part I: Observations, Journal of the atmospheric sciences, 63, 2212–2230, 2006.

Knutson, T. R. and Manabe, S.: Time-mean response over the tropical Pacific to increased c0 2 in a coupled ocean-atmosphere model, Journal of Climate, 8, 2181–2199, 1995.

Landsea, C. W.: A climatology of intense (or major) Atlantic hurricanes, Monthly weather review, 121, 1703–1713, 1993.

Lebel, T. and Ali, A.: Recent trends in the Central and Western Sahel rainfall regime (1990–2007), Journal of hydrology, 375, 52–64, 2009.

Liu, W., Cook, K. H., and Vizy, E. K.: The role of mesoscale convective systems in the diurnal cycle of rainfall and its seasonality over sub-Saharan Northern Africa, Climate Dynamics, 52, 729–745, 2019.

Martin, E. R. and Thorncroft, C.: Representation of African easterly waves in CMIP5 models, Journal of Climate, 28, 7702–7715, 2015.

McCrary, R. R., Randall, D. A., and Stan, C.: Simulations of the West African monsoon with a superparameterized climate model. Part II: African easterly waves, Journal of Climate, 27, 8323–8341, 2014.

Monerie, P.-A., Wainwright, C. M., Sidibe, M., and Akinsanola, A. A.: Model uncertainties in climate change impacts on Sahel precipitation in ensembles of CMIP5 and CMIP6 simulations, Climate Dynamics, 55, 1385–1401, 2020.

Nesbitt, S. W., Cifelli, R., and Rutledge, S. A.: Storm morphology and rainfall characteristics of TRMM precipitation features, Monthly Weather Review, 134, 2702–2721, 2006.

Nicholson, S. E.: The West African Sahel: A review of recent studies on the rainfall regime and its interannual variability, International Scholarly Research Notices, 2013, 453 521, 2013.

Núñez Ocasio, K., Davis, C., Moon, Z., and Lawton, Q.: Moisture dependence of an African easterly wave within the West African monsoon system, Journal of Advances in Modeling Earth Systems, 16, e2023MS004 070, 2024.

https://doi.org/10.5194/egusphere-2026-2879
Preprint. Discussion started: 11 June 2026

Núñez Ocasio, K. M., Dougherty, E. M., Moon, Z. L., and Davis, C. A.: Response of African Easterly Waves to a Warming Climate: A Convection-Permitting Approach, Journal of Advances in Modeling Earth Systems, https://doi.org/10.1029/2025MS005146, 2025.

O'Neill, B. C., Tebaldi, C., Van Vuuren, D. P., Eyring, V., Friedlingstein, P., Hurtt, G., Knutti, R., Kriegler, E., Lamarque, J.-F., Lowe, J., et al.: The scenario model intercomparison project (ScenarioMIP) for CMIP6, Geoscientific Model Development, 9, 3461–3482, 2016.

Panthou, G., Lebel, T., Vischel, T., Quantin, G., Sane, Y., Ba, A., Ndiaye, O., Diongue-Niang, A., and Diopkane, M.: Rainfall intensification in tropical semi-arid regions: the Sahelian case, Environmental Research Letters, 13, 064 013, 2018.

Pytharoulis, I. and Thorncroft, C.: The low-level structure of African easterly waves in 1995, Monthly Weather Review, 127, 2266–2280, 1999.

Rackow, T., Pedruzo-Bagazgoitia, X., Becker, T., Milinski, S., Sandu, I., Aguridan, R., Bechtold, P., Beyer, S., Bidlot, J., Boussetta, S., et al.: Multi-year simulations at kilometre scale with the Integrated Forecasting System coupled to FESOM2. 5 and NEMOv3. 4, Geoscientific Model Development, 18, 33–69, 2025.

Raj, J., Bangalath, H. K., and Stenchikov, G.: Future projection of the African easterly waves in a high-resolution atmospheric general circulation model, Climate Dynamics, 61, 3081–3102, 2023.

Ruti, P. M. and Dell'Aquila, A.: The twentieth century African easterly waves in reanalysis systems and IPCC simulations, from intra-seasonal to inter-annual variability, Climate dynamics, 35, 1099–1117, 2010.

Segura, H., Pedruzo-Bagazgoitia, X., Weiss, P., Müller, S. K., Rackow, T., Lee, J., Dolores-Tesillos, E., Benedict, I., Aengenheyster, M., Aguridan, R., et al.: nextGEMS: entering the era of kilometer-scale Earth system modeling, EGUsphere, 2025, 1–39, 2025.

Skinner, C. B. and Diffenbaugh, N. S.: Projected changes in African easterly wave intensity and track in response to greenhouse forcing, Proceedings of the National Academy of Sciences, 111, 6882–6887, 2014.

Sylla, M. B., Diallo, I., and Pal, J.: West African monsoon in state-of-the-science regional climate models, in: Climate variability-regional and thematic patterns, IntechOpen, 2013.

Takasuka, D., Becker, T., and Bao, J.: Precipitation Characteristics and Thermodynamic-Convection Coupling in Global Kilometer-Scale Simulations, Journal of Advances in Modeling Earth Systems (submitted), https://www.authorea.com/doi/full/10.22541/essoar.174834999.93788721/v1?commit=cddb48745c141db7e116610bffc6b46b826eaa00, 2025.

Thorncroft, C. and Blackburn, M.: Maintenance of the African easterly jet, Quarterly Journal of the Royal Meteorological Society, 125, 763–786, 1999.

Thorncroft, C. D. and Hoskins, B. J.: An idealized study of African easterly waves. I: A linear view, Quarterly Journal of the Royal Meteorological Society, 120, 953–982, 1994.

Thorncroft, C. D., Hall, N. M. J., and Kiladis, G. N.: Three-Dimensional Structure and Dynamics of African Easterly Waves. Part III: Genesis, Journal of the Atmospheric Sciences, 65, 3596–3607, https://doi.org/10.1175/2008JAS2575.1, 2008.

Ventrice, M. J., Thorncroft, C. D., and Janiga, M. A.: Atlantic tropical cyclogenesis: A three-way interaction between an African easterly wave, diurnally varying convection, and a convectively coupled atmospheric Kelvin wave, Monthly weather review, 140, 1108–1124, 2012.

Vizy, E. K. and Cook, K. H.: Mechanisms by which Gulf of Guinea and eastern North Atlantic sea surface temperature anomalies can influence African rainfall, Journal of Climate, 14, 795–821, 2001.

Vizy, E. K. and Cook, K. H.: Development and application of a mesoscale climate model for the tropics: Influence of sea surface temperature anomalies on the West African monsoon, Journal of Geophysical Research: Atmospheres, 107, ACL–2, 2002.

https://doi.org/10.5194/egusphere-2026-2879
Preprint. Discussion started: 11 June 2026

720 White, B. et al.: The Role of Orography in African Easterly Wave Development, Monthly Weather Review, 149, 3215–3235, https://doi.org/10.1175/MWR-D-20-0313.1, 2021.

	ERA5	**Historical Simulation**	**Future Projection**
Number of AEW days	1770	1638	2019
Number of Non AEW days	1890	2022	1641

Table 1. Comparison of AEW and non-AEW days in ERA5, historical and future simulations

https://doi.org/10.5194/egusphere-2026-2879
Preprint. Discussion started: 11 June 2026

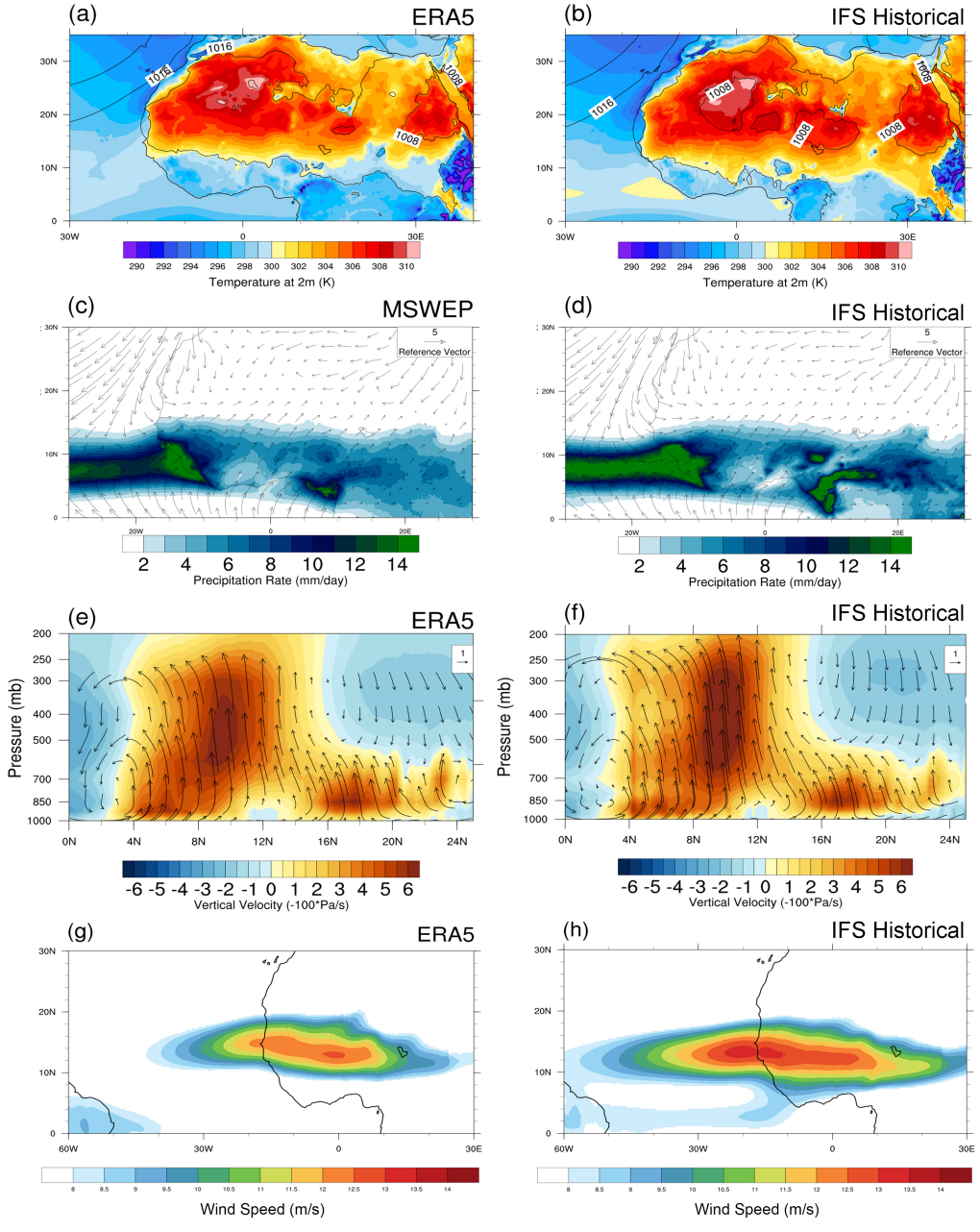

Figure 1. Mean JJAS fields in the observations (left column) and in the IFS model (right column): surface temperature (K, shaded) and sea level pressure (hPa, contours) (a,b); total precipitation (mm/day, shaded) and surface winds (m/s, vectors) (c,d); vertical-cross section zonally averaged between 20ºW-30ºE of omega (in 10^{-2} Pa/s with a change of sign where positive values represent upward motion, shaded) and omega-meridional wind vectors (m/s for meridional wind while omega is scaled to match the magnitude of the meridional wind, vectors) (e,f); wind speed at 600 hPa (g,h). In the left column, all variables are derived from ERA5 except for precipitation, for which MSWEP dataset was used.

https://doi.org/10.5194/egusphere-2026-2879
Preprint. Discussion started: 11 June 2026

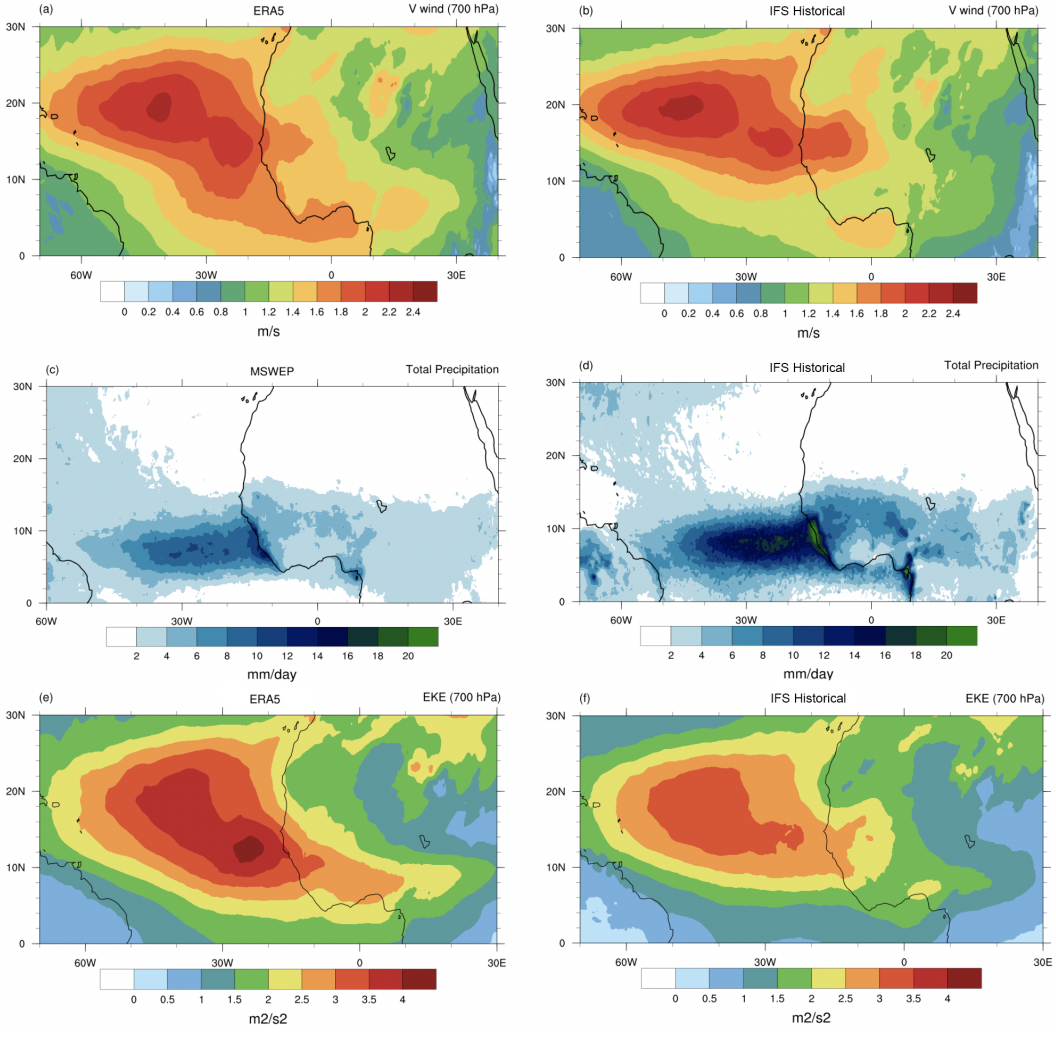

Figure 2. Variability associated with AEW in ERA5 reanalysis (left column) and IFS model (right column). Standard deviation of band-pass filtered fields between 3 to 5 days during JJAS season of: meridional wind at 700 hPa (m/s) (a,b); precipitation (mm/day) (c,d); eddy kinetic energy at 700 hPa (m^2/s^2) (e,f).

https://doi.org/10.5194/egusphere-2026-2879
Preprint. Discussion started: 11 June 2026

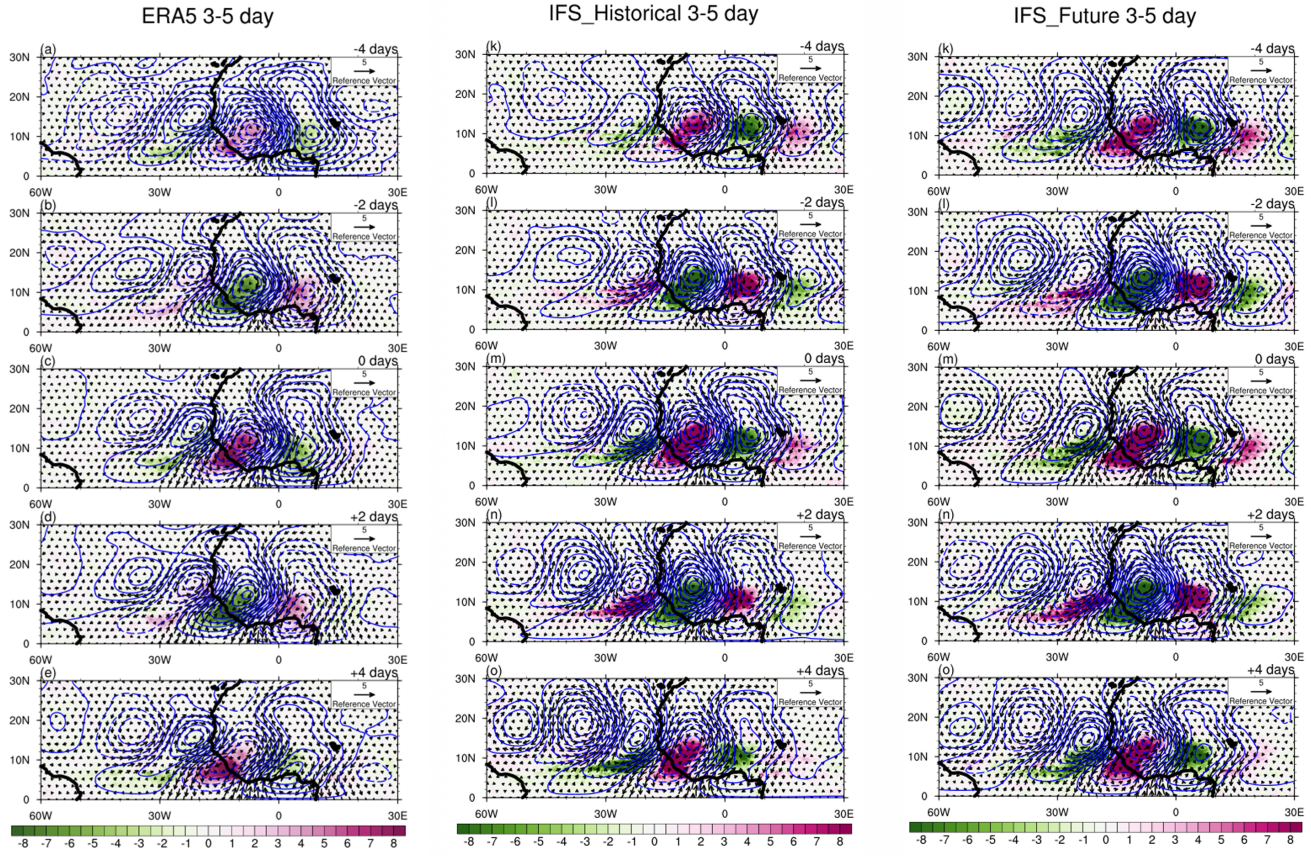

Figure 3. Representation of horizontal structure of AEWs at 700 hPa in observations and reanalysis (left column), IFS historical simulation (middle column) and IFS projection (right column): composite analysis of anomalous wind vectors (m/s), rainfall (mm/day) and stream lines using the dates when the meridional wind at 700 hPa and the base point (1°W and 11.5°) is above the 90 percentile minus those at dates for which it is below the 10 percentile (c,h,m); same composite analysis was performed for 4 days before (a,f,k), 2 days before (b,g,l), 2 days after (d,i,n) and 4 days after (e,j,o).

https://doi.org/10.5194/egusphere-2026-2879
Preprint. Discussion started: 11 June 2026

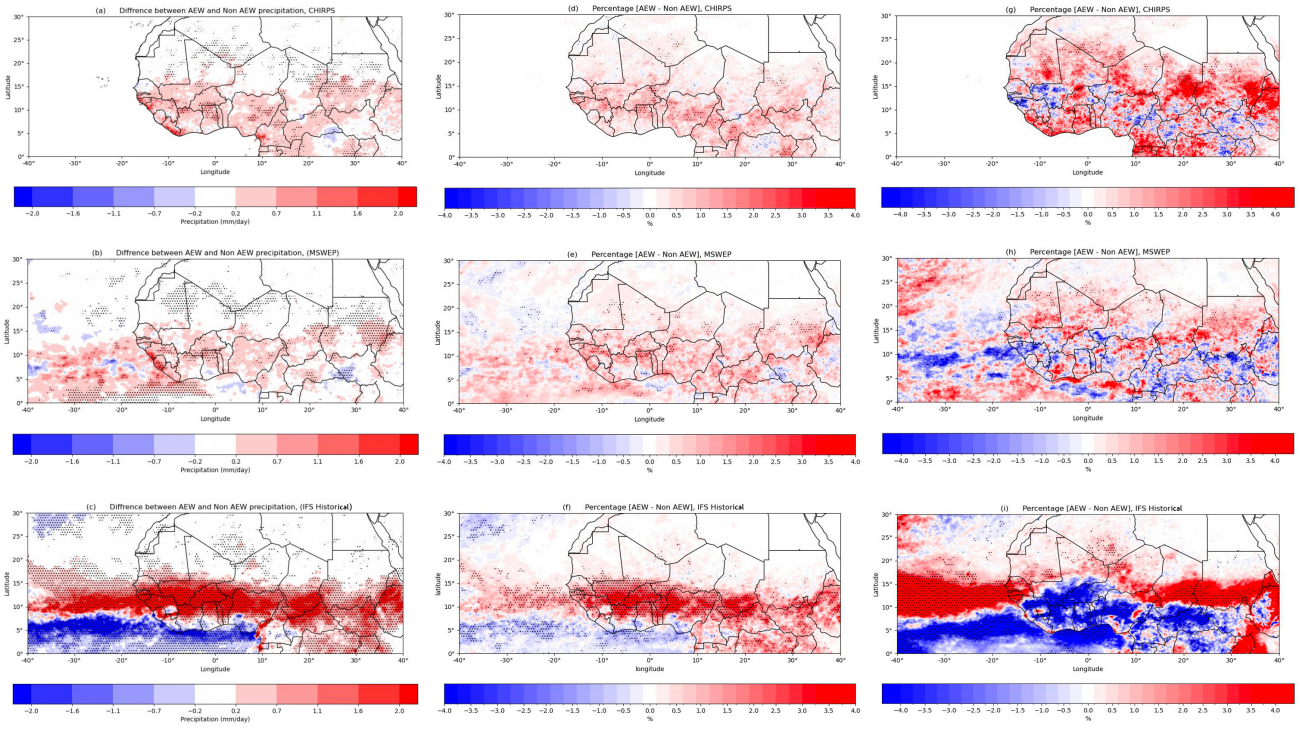

Figure 4. Differences in rainfall characteristics between AEW days and non-AEW days in CHIRPS (top row), MSWEP (middle row) and IFS historical simulation (bottom row) for mean JJAS rainfall (mm/day) (a,b,c), ratio of extreme days (defined as those above the 95 percentile of rainy days) to total days in the category (AEW or non-AEW days) (difference in percentage) (d,e,f); ratio of moderate days (defined as those below the 75 percentile of rainy days) to total days in the category (AEW or non-AEW days) (difference in percentage) (g,h,i). Stippling indicates regions where the p value of the local null hypothesis of equal means is below 0.05.

https://doi.org/10.5194/egusphere-2026-2879
Preprint. Discussion started: 11 June 2026

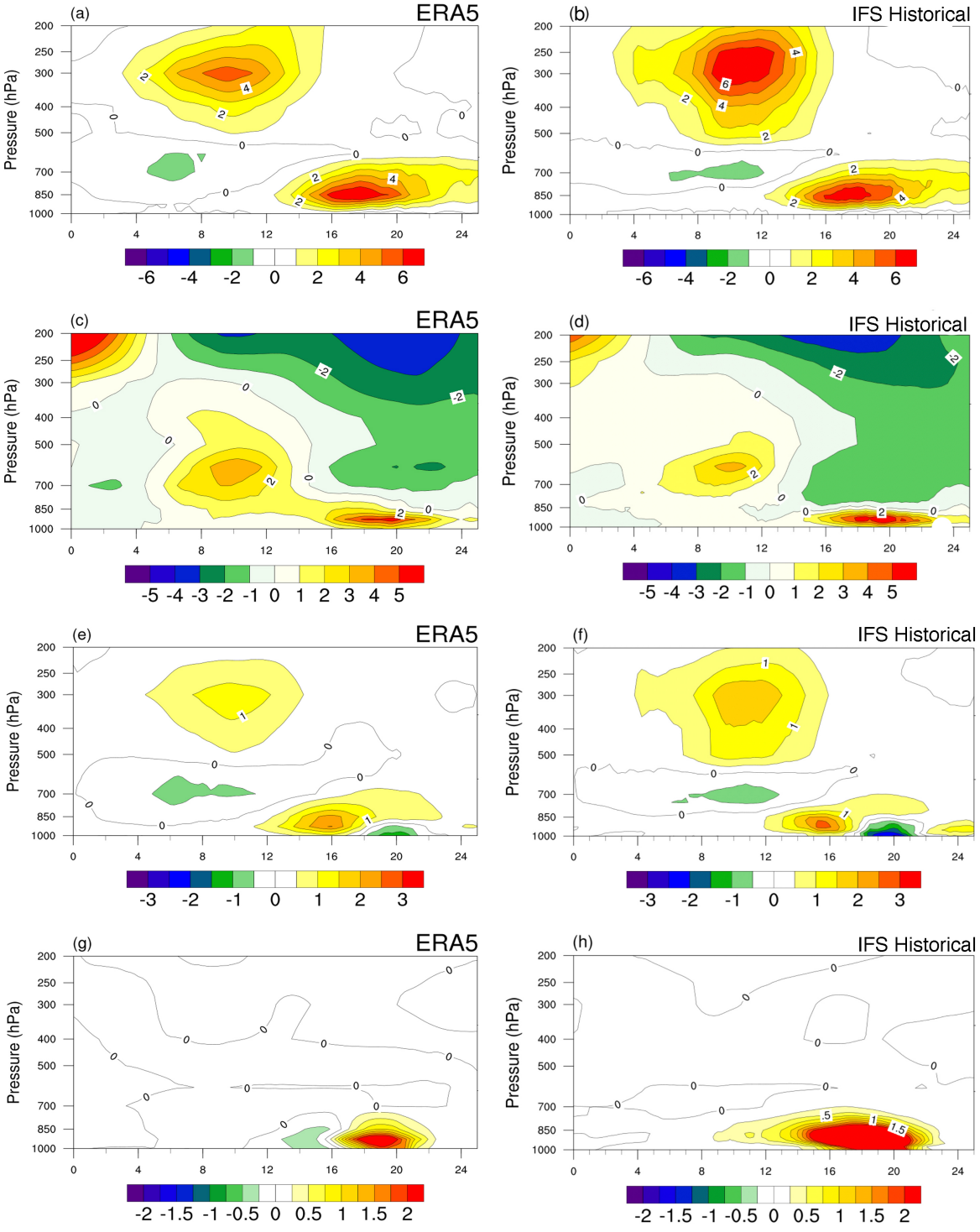

Figure 5. AEW energy conversion terms (m^2/s^2/day) in ERA5 (left column) and the IFS historical simulation (right column): JJAS mean meridional height cross-sections zonally averaged between 20ºW and 30ºW of 3–5 day baroclinic conversion (C_{pk}) (a,b), barotropic conversion (C_k) (c,d), diabatic generation of eddy available potential energy (G_E) (e,f), and conversion from zonal mean to eddy potential energy (C_A) (g,h)

https://doi.org/10.5194/egusphere-2026-2879
Preprint. Discussion started: 11 June 2026

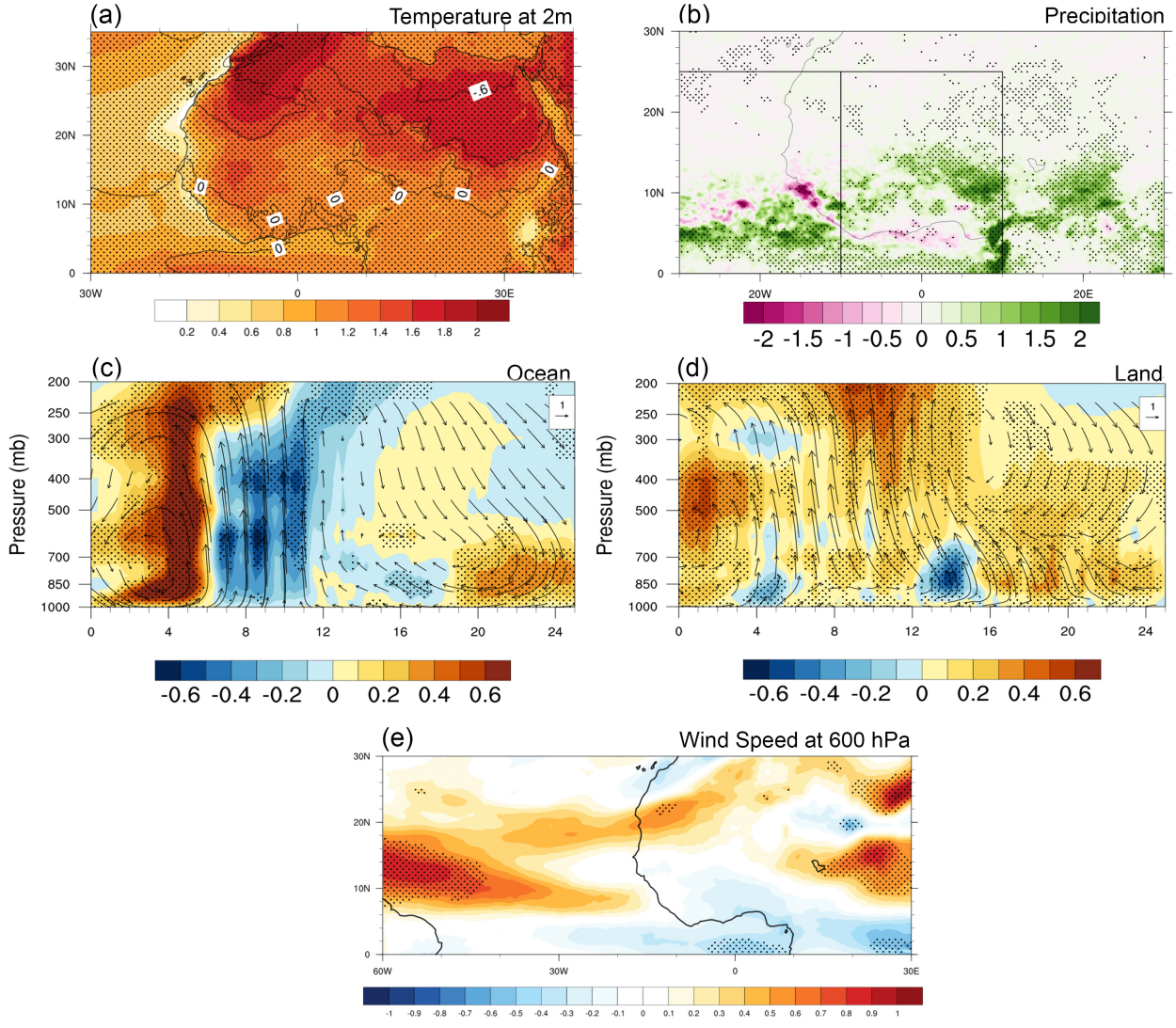

Figure 6. Projected changes in mean fields. Difference between JJAS means in the projection and historical simulations of: 2 m temperature (K) (a), precipitation (mm/day) (b), the boxes in (b) represents where the zonal averaging is performed for (c) and (d), meridional cross-section of omega (in 10^{-2} Pa/s with a change of sign where positive values represent upward motion, shaded) over the ocean (c) and over land (d), and wind speed at 600 hPa (m/s). To ease comparison, plots c and d show as vectors the climatological JJAS means in IFS historical simulation of omega-meridional wind vectors (m/s for meridional wind while omega is scaled to match the magnitude of the meridional wind). Stippling mark regions where the p value of the local null hypothesis of equal means is below 0.05.

https://doi.org/10.5194/egusphere-2026-2879
Preprint. Discussion started: 11 June 2026

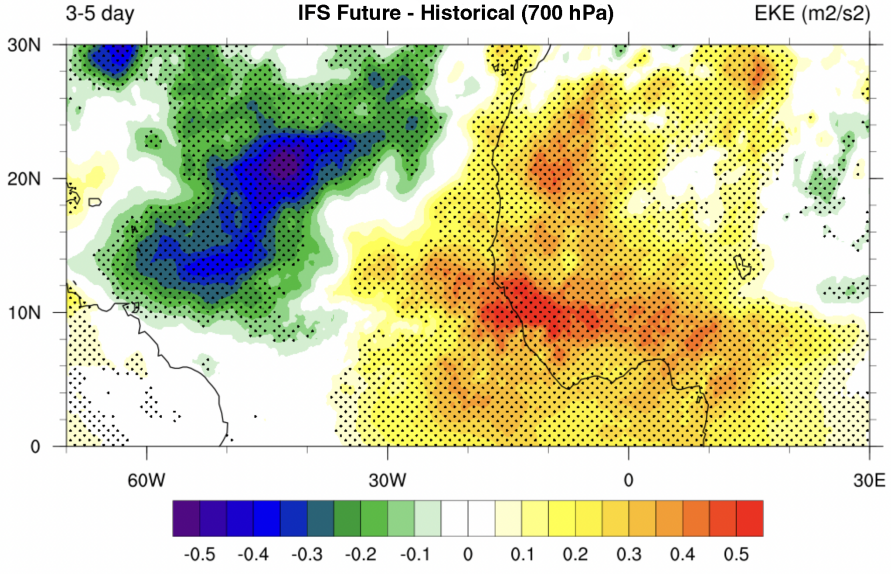

Figure 7. Projected change in AEW activity. Differences between JJAS 3-5 day EKE at 700 hPa in the projection and historical simulations (m^2/s^2). Stippling mark regions where the p value of the local null hypothesis of equal means is below 0.05.

https://doi.org/10.5194/egusphere-2026-2879
Preprint. Discussion started: 11 June 2026

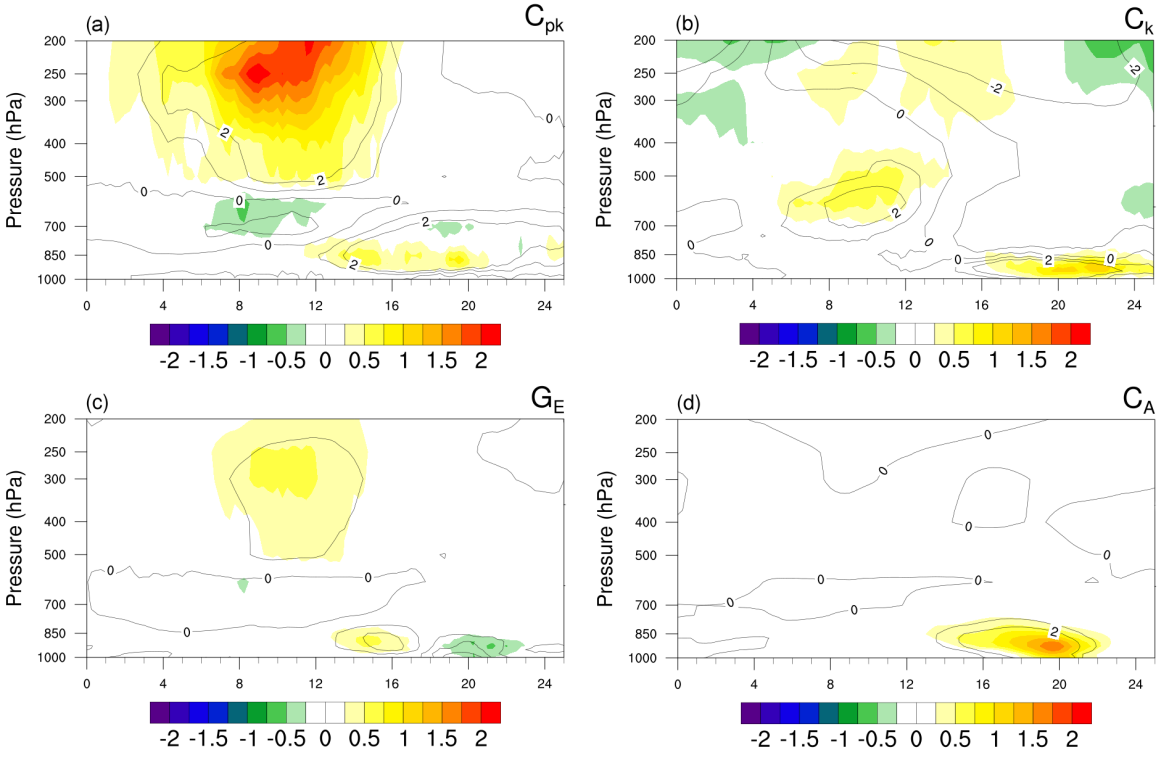

Figure 8. Projected changes in AEW energy conversion terms (m^2/s^2/day). Difference between JJAS means in the projection and historical simulations of JJAS mean meridional height cross-sections zonally averaged between 20ºW and 30ºW of 3–5 day baroclinic conversion (C_{pk}) (a), barotropic conversion (C_k) (b), diabatic generation of eddy available potential energy (G_E) (c), and conversion from zonal mean to eddy potential energy (C_A) (d). The contours represent historical values of each term.

https://doi.org/10.5194/egusphere-2026-2879
Preprint. Discussion started: 11 June 2026

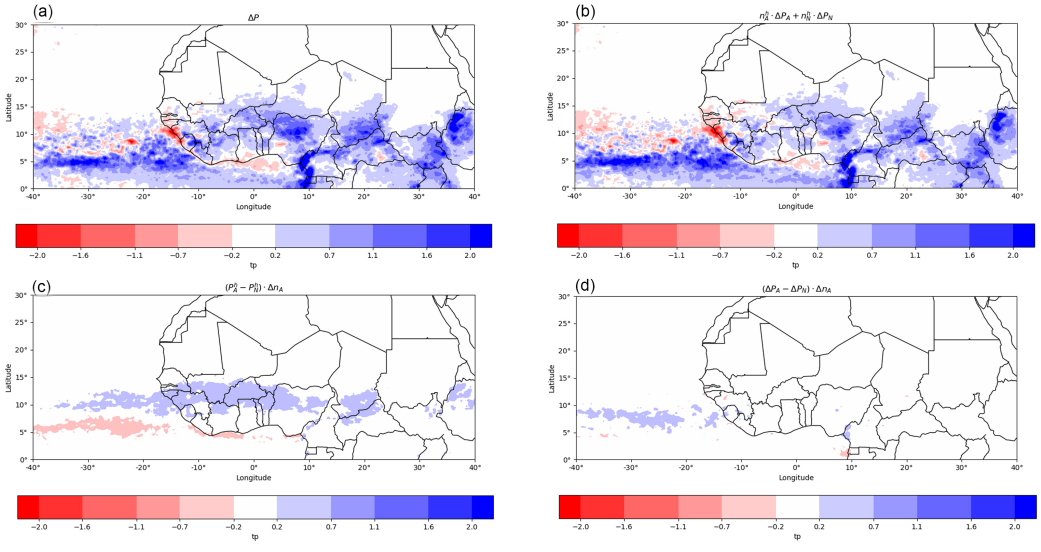

Figure 9. Decomposition of projected changes in JJAS mean precipitation (a) into a term coming from the change in mean precipitation during both AEW and non-AEW days ($n_A^h \cdot \Delta P_A + n_N^h \cdot \Delta P_N$) (b), the contribution from changes in the number of AEW days ($(P_A^h - P_N^h) \cdot \Delta n_A$) (c) and the cross-product term ($(\Delta P_A - \Delta P_N) \cdot \Delta n_A$) (d). Units are mm/day.

https://doi.org/10.5194/egusphere-2026-2879
Preprint. Discussion started: 11 June 2026

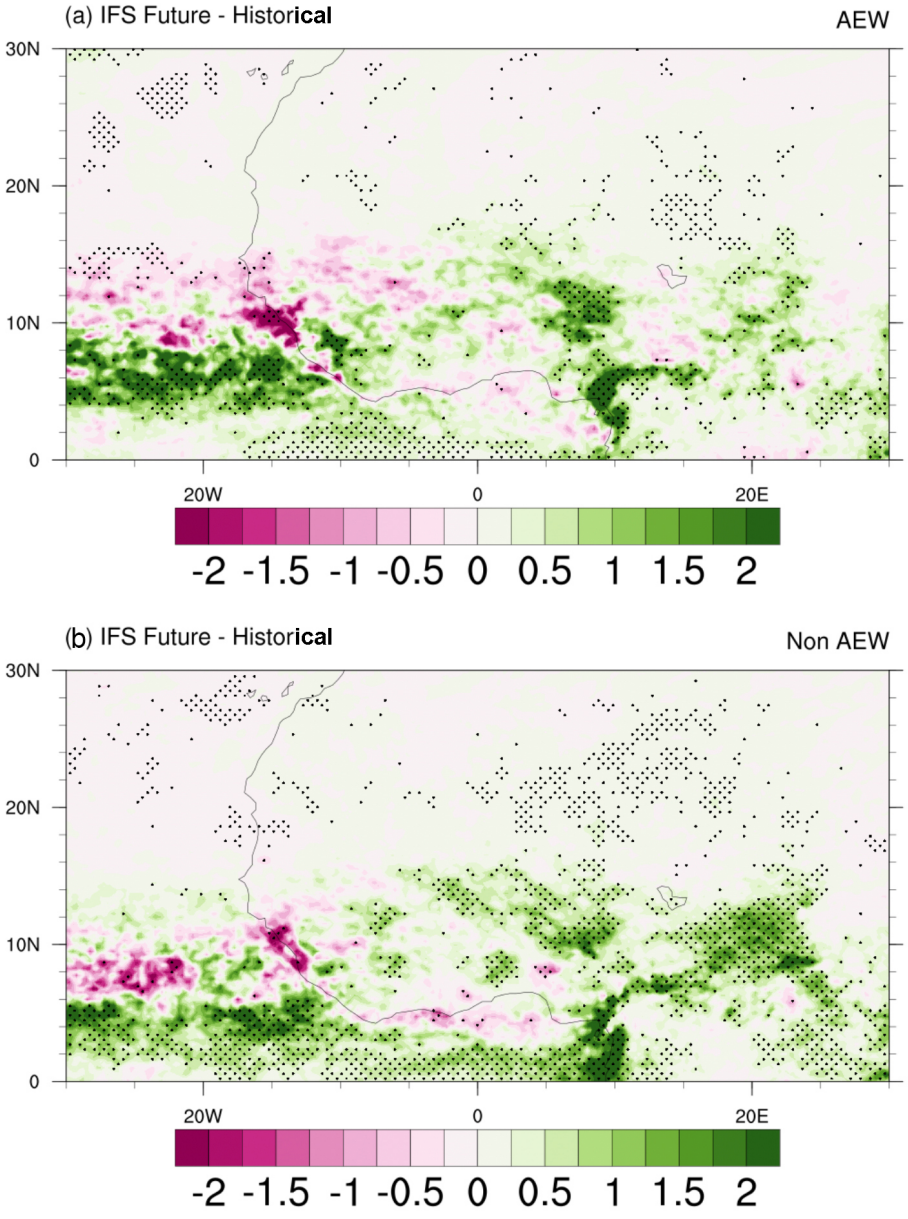

Figure 10. Differences in mean JJAS precipitation between the projection and the historical simulation taking only into account AEW days (a) and non-AEW days (b). Units are mm/day. Stippling marks regions where the p value of the local null hypothesis of equal means is below 0.05.

https://doi.org/10.5194/egusphere-2026-2879
Preprint. Discussion started: 11 June 2026

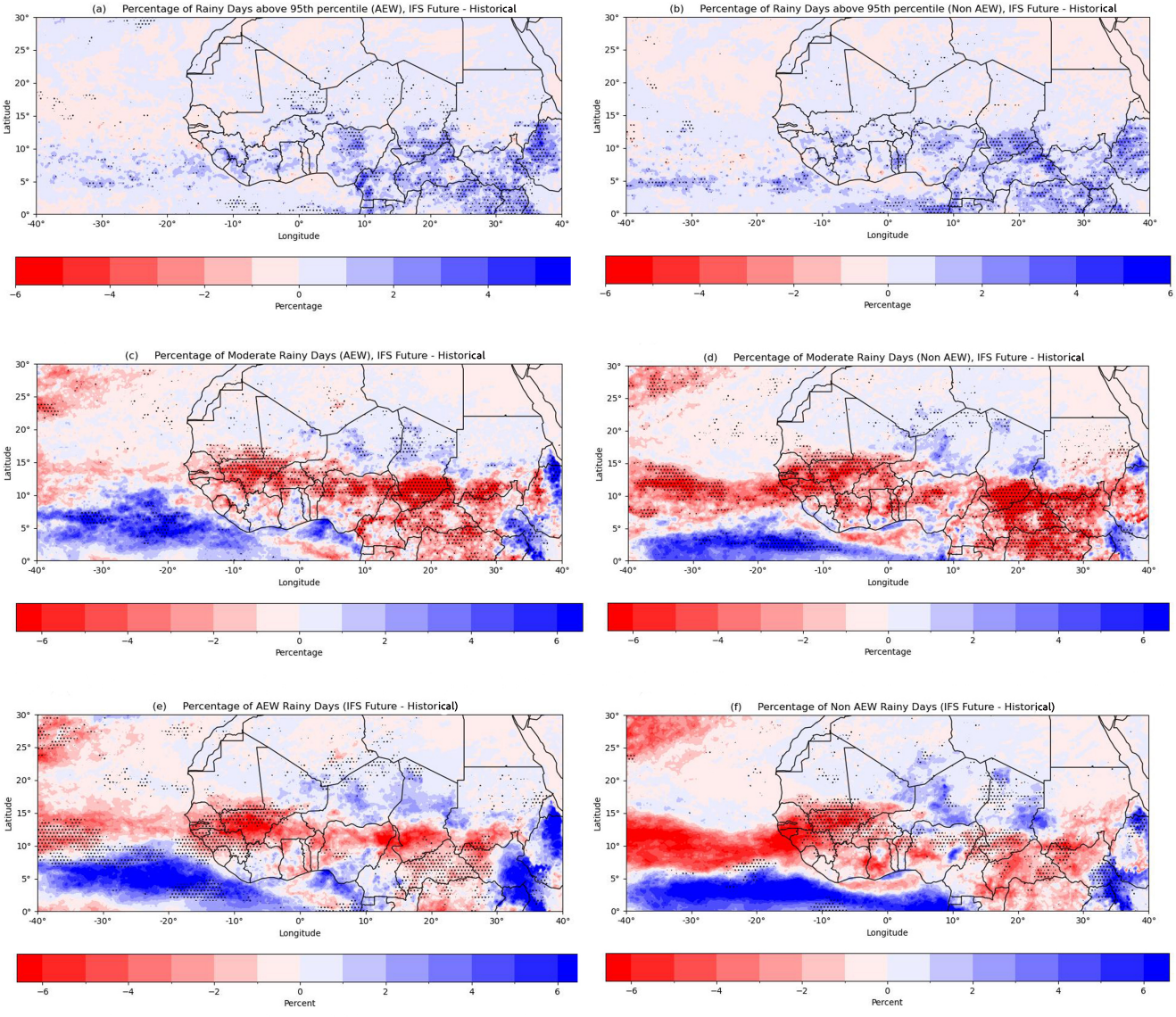

Figure 11. Projected changes in JJAS precipitation characteristics separated into AEW days (left column) and non-AEW days (right column): percentage of extreme rainfall events (a,b), percentage of moderate rainfall events (c,d), percentage of rainy days (e,f). Units are differences in percentages. Stippling marks regions where the p value of the local null hypothesis of equal means is below 0.05.

https://doi.org/10.5194/egusphere-2026-2879
Preprint. Discussion started: 11 June 2026

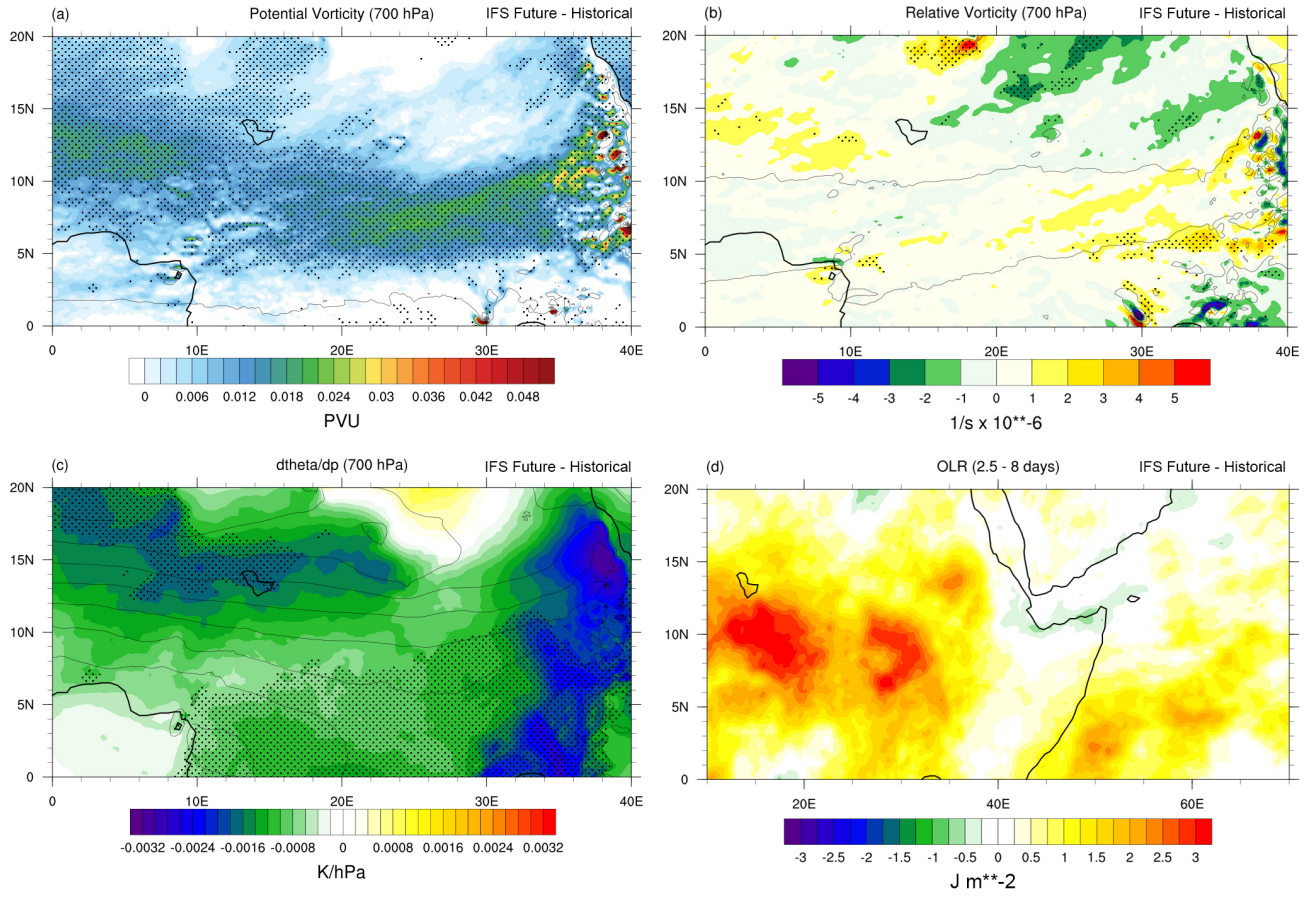

Figure 12. Projected changes in AEWs in factors related to the genesis and amplification of AEWs. Differences in JJAS means of potential vorticity (a), relative vorticity ($10^{-6}s^{-1}$) (b) and static stability (K/hPa) (c). Panel d shows the 2.5-8 days variability of OLR (W/m^2). Stippling in plots a-c mark regions where the p value of the local null hypothesis of equal means is below 0.05.